Torque Control in Field Weakening Mode

Master Thesis
Group PED4-1038C

Institute of Energy Technology
Aalborg University

03^{rd} June 2009

Board of Studies of Energy

Title:	Torque Control in Field Weakening Mode
Semester:	4^{th}
Semester theme:	
Project period:	01.02.09 to 03.06.09
ECTS:	30
Supervisors:	Peter O. Rasmussen
	Torben N. Matzen
Project group:	PED4-1038C

SYNOPSIS:

This project deals with the control of an IPMSM. The objective of the project is to implement and investigate a control structure that is able to drive the motor in Field Weakening(FW) mode. In order to reach this objective, first a Field Oriented Control structure is implemented in Matlab/Simulink with a Maximum Torque per Ampere control. Then a FW control algorithm that acts on the angle of the stator current vector is investigated and implemented in the overall simulation model. The presented simulation results prove that the implemented method is capable of FW, with good speed and torque dynamics. The designed control is then implemented in a dSpace control system. The experimental results that are presented at the end confirm the fact that the FOC is working, and is capable of FW regime.

Călin Căpitan

Copies:	- 3
Pages, total:	- 68
Appendix:	- 3
Supplements:	- 3 CDs

By signing this document, each member of the group confirms that all participated in the project work and thereby all members are collectively liable for the content of the report.

Preface

The present report is prepared by Group PED4-1038C in the 4^{th} Semester M.Sc., at Power Electronics and Drives, Aalborg University. The project, with the title *Torque Control in Field Weakening Mode*, is a proposal from Danfoss. The main idea of the project is to control the speed and torque of an Interior Permanent Magnet Synchronous Machine(IPMSM) in the flux weakening regime, considering the voltage and current limits of the inverter .

The project is documented in a main report and appendixes. The main report can be read as a self-contained work, while the appendixes contain details about mesurements, data sheets, or other information. In this project the chapters are consecutive numbered whereas the appendixes are labeled with letters.

Figures, equations and tables are numbered in succession within the chapters. For example, Fig.2.3 is the third figure in chapter 2.

The references are written with the Harvard method with [Author,Year]. More detailed information about the sources is given at the end of the main report in Bibliography.

Matlab/Simulink is used for all the simulations. For implementation in the real time system a dSpace setup is used. The software used as an interface between the user and dSpace is Control Desk.

A CD-ROM containing the main report and appendixes is attached to the project.

I would like to thank Torben N. Matzen, for his support in helping me with all the problems that I confronted with. I would also like to thank Walter Neumayr and the technical staff from IET for their help in building the experimental setup.

The author

Contents

List of Figures

1 Introduction

This chapter begins with a short introduction into the Field Weakening mode of an IPMSM. The main features of this control are presented, taking into account also the inverter that is feeding the machine. Next the Problem formulation and the Objective of this project are stated. In the end, the limitations and the structure of this report are presented.

1.1 Task background

Recently, the Interior Permanent Magnet Synchronous Machine (IPMSM) is getting more and more popular in applications like traction and machine spindle drives, air conditioning compressors, electrical vehicles, integrated starters/alternators. The reason why the IPMSM is getting more attention is due to its attractive characteristics like high efficiency, high power density, high torque/inertia ratio, wide speed operation range, and free from maintenance.[Ching,2005]
In traction and spindle drives, where the motor is supposed to work at constant power for a wide speed range, the high saliency IPMSM is most suited.[Sul,2003]

In order to have a high performance drive using an IPMSM, the control strategy chosen has to highlight all the advantages that this kind of permanent magnet (PM) motor has. Indirect Field Oriented Control(FOC) is one of the best solutions for a high performance drive when having an IPMSM. One of the most used linear control strategies, for FOC, is to keep the d axis current i_{s_d}=0, so that the produced torque is proportional to the q current component i_{s_q}, like in Eq.1.1

$$T_e = \frac{3}{2} p_b \Psi_m i_{s_q} \tag{1.1}$$

$$T_e = \frac{3}{2} p_b (\Psi_m i_{s_q}) + \frac{3}{2} p_b (L_d - L_q) i_{s_q} i_{s_d} \tag{1.2}$$

Although this is a straightforward method, by setting i_{s_d}=0, the potential reluctance torque of the IPMSM is not employed(Eq.1.2). On the other hand a nonlinear method can be used to take advantage of the reluctance torque. Depending on the objective, unity power factor control, constant flux linkage control, maximum torque per ampere control(MTPA) or maximum efficiency control can be implemented.[Ching,2005].

When using one of the above control techniques, the speed of the motor is increased up to the base speed. To fully utilize the wide-speed capabilities of the IPMSM, and to

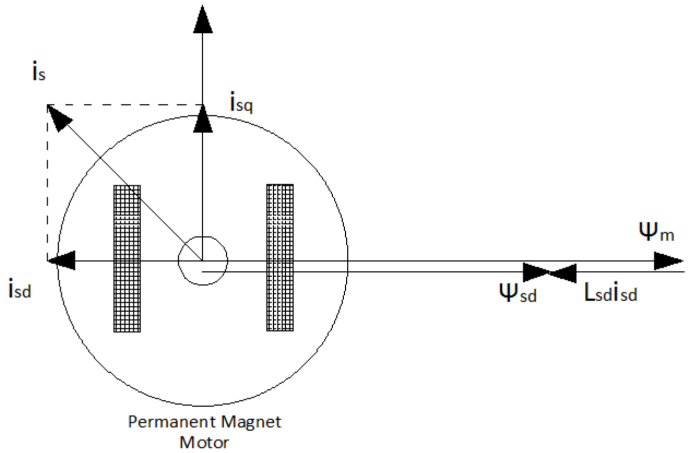

Figure 1.1: *Vector diagram illustrating the resulting flux linkage[Soong,1994]*

further increase the speed, a Field-Weakening Algorithm (FWA) has to be introduced. The action of a field-weakening procedure is to lower the influence of the permanent magnets flux linkage, Ψ_m, on the resulting air-gap flux. This is done by increasing the absolute value of the d(magnetizing axis) stator current component i_{s_d}, towards the negative side [Morimoto,1990]Fig.1.1.

$$\Psi_{s_d} = L_{s_d} \cdot i_{s_d} + \Psi_m \tag{1.3}$$

When the absolute value of the the d component (flux component) of the stator current is increased, the resulting air gap flux is lowered. This causes the speed of the motor to increase also. As the motor speed increases above the base speed, in field weakening mode, the maximum current and voltage limits of the inverter are reached. So the FWA has to take also into consideration the current and voltage limits of the inverter. These limits can be expressed in the (i_{s_d},i_{s_q}) plane. The current limit is expressed as a circle with fixed radius, while the voltage limit is described as an ellipse. The radius of the ellipse is getting smaller as the speed of the motor is increasing, as it is shown in Fig.1.2.

When the speed of the motor is equal to the base speed, (point B in Fig.1.2), the maximum voltage and current that the inverter can supply are reached. The speed can be further increased by going into field weakening, which means that the applied voltage is kept constant or lowered (depending on the constant power working capabilities of the machine) while the current magnitude remains constant and equal to its maximum value. Ideally the current vector follows the current limit circle path(line BC in Fig.1.2). The maximum speed that can be reached in field weakening, while keeping the output power constant depends on the saliency ratio ($\xi = \frac{L_q}{L_d}$), and on the flux linkage of the permanent magnets Ψ_m [Soong,1994].

There are several methods proposed in literature that deal with flux weakening, taking into account also the inverter limits(voltage and current). The main challenge for an FOC control, is how to generate the reference current commands i_d* and i_q*, from the speed command, that can follow the BC(field weakening)curve in Fig.1.2.

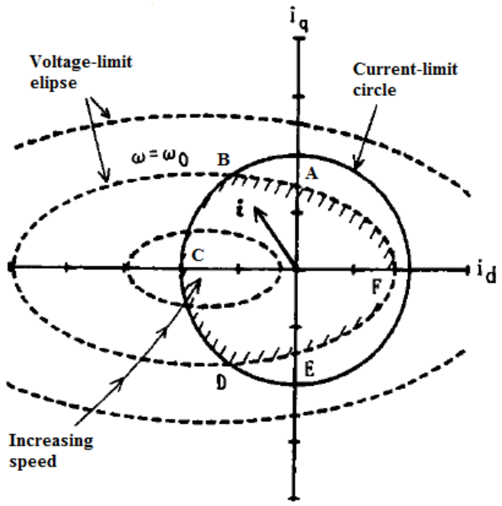

Figure 1.2: *dq representation of the inverter voltage and current limits[Morimoto,1990]*

1.2 Problem formulation

The IPMSM motor is capable of speeds above the base speed, in field weakening mode while keeping the output power constant. During field weakening, the motor is running at the maximum available current from the inverter, while the maximum available voltage is getting smaller. At one point, while using a FOC method to run the motor, there is a high potential of saturating the PI current controllers. If the controllers saturate, the control over the motor is lost.

The problem is then: *How to generate the reference currents for the control in field weakening, so that the saturation of the current controllers is overcome.*

1.3 Objective

The project 'Torque Control in Field Weakening Mode' is a proposal from Danfoss. It deals with the control of an Interior Permanent Magnet Synchronous Motor. The objective of this project is to implement a Field Oriented Control capable of Field Weakening, taking into consideration the inverter limits, and to investigate the dynamics of the controllers while running the motor in field weakening mode.

Aims of the project:

- gain knowledge about the field weakening methods for IPMSM
- implement an FOC method capable of field weakening in Matlab/Simulink
- test the performance and dynamics of the control in a real-time system (dSpace)

.

1.4 Project limitation

In order to reach the objective of the project, some constraints and limitations were applied:

- The variation of the L_d and L_q inductance due to saturation or current variation is neglected, when deriving the MTPA curve of the motor.
- The modulation used, Space Vector Modulation, is not investigated; an existing model, from the dSpace laboratory was used.
- There is no information regarding the nominal operating point of the Sauer-Danfoss motor used for this project.

1.5 Report Structure

The present report is structured in five chapters. A theoretical background on the topic Field Weakening, is presented in the introductory first chapter. In this chapter, the problem formulation, the objective and the limitations of the project are stated. The second chapter presents the main features of the interior permanent magnet synchronous machine, together with the mathematical model of the machine. Based on the mathematical model, a Matlab/Simulink model of the machine is made and presented. In Chapter3 the design, simulation model and results of the Field Oriented Control algorithm capable of Field Weakening is prsented. The laboratory implementation of the control in dSpace is presented in Chapter4. The report conclusions are drawn in the final chapter.

2

Permanent Magnet Synchronous Motor

This chapter begins with a classification of the Permanent Magnet machines. Then the main characteristics of the Interior type permanent magnet motor are presented, together with the electrical parameters of the IPMSM used in this project. Next the mathematical model of the IPMSM is presented. Based on the mechanical model of the machine, a dynamic simulation model is made using Matlab/Simulink. In the end of the chapter the measurements made to calculate the mechanical parameters of the machine and the results from the simulation model are presented.

2.1 Introduction

Permanent Magnet Synchronous Motors (PMSM) are attracting growing attention for a wide variety of industrial applications, from simple applications like pumps or fans to high-performance drives like machine-tool servos. This is due to their main characteristics: high power density, high torque to inertia ratio and high efficiency.[Morimoto,1990] Permanent magnet motors are double excited electric machines. The first source of excitation is the field of the permanent magnet situated in the rotor, while the second source is the field produced by the stator winding when supplied with a 3-phased voltage system.

In comparison with the conventional synchronous machines, where the rotor field is also produced by an electric winding, the PMSM has no wires in the rotor, which reduces the copper losses of the machine. Also due to the lack of rotor windings there is no need for brushes and slip-rings. Taking all this into account, a PMSM machine has a smaller size and a higher efficiency, for a given power, compared to a conventional synchronous machine.[PED8]. On the other hand, the field produced by the permanent magnets is constant and cannot be controlled as easy as the conventional doubly electric excited machines, by changing the field current.[Chandana,2002]

The PM machines can be classified as in the diagram presented in Fig.2.1[Chandana,2002].

First, depending on the nature of the stator field excitation, the PM machines can be classified as PM with D.C. excitation(PMDC)or PM with A.C. excitation(PMAC). The PMDC motor has the same configuration as the conventional DC machine, having a stator winding with brushes and comutator, except for the rotor, where the rotor (field) winding was replace with permanent magnets. The PMAC machine is a synchronous machine, with no brushes or comutator.

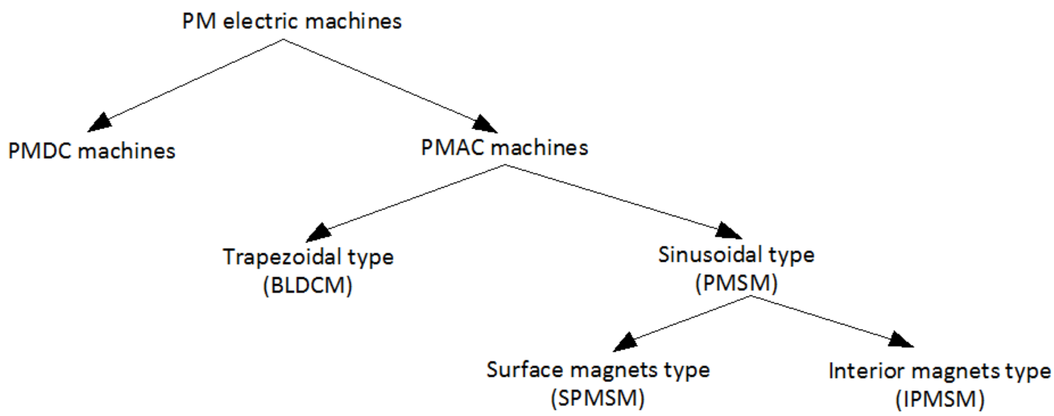

Figure 2.1: *Permanent magnet machines classification[Chandana,2002]*

Further, depending on the type of back-EMF voltage induced in the stator windig, the PMAC machines can be classified as trapezoidal-type PMAC machines or sinusoidal-type PMAC machines. The trapezoidal PMAC machine, also called brushless DC machine(BLDCM), is excited form a rectangular current waveform, whereas the sinusoidal type requires AC stator excitation. The presence of torque ripples in an trapezoidal-type PMAC machine, and also due to the development of vector control for AC drives has encouraged the usage of sinusoidal PMAC, also known as PM synchronous machines(PMSM).[Chandana,2002]

The PMSM can be classified into two types, depending on the positioning of the magnets in the rotor of the machine. These are the surface mounted PM machine (SMPMSM) and interior mounted PM machine (IPMSM), like presented in Fig.2.2

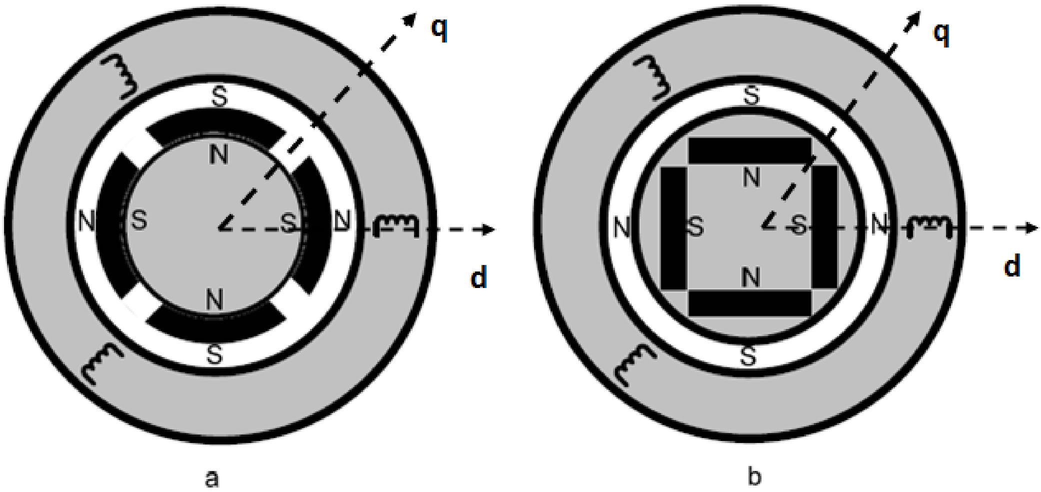

Figure 2.2: *Cross section showing the differences between the SMPMSM and the IPMSM[PED8]*

For the SPMSM the magnets are placed on the surface of the rotor core Fig.2.2a, while for the IPMSM the magnets are buried in the rotor core Fig.2.2b. As shown in Fig.2.2, the magnetic flux induced by the magnets defines the rotor direct axis, *d*, (magnetization axis) through the center line of the magnets. The rotor quadrature, *q*, axis is situated at 90 electrical degrees, from the d axis. For the interior PMSM the d axis air gap is increased compared to the q axis air gap, due to the fact that the relative permeability of the permanent magnets is close to 1, which is the relative permeability of air. So, for the IPMSM the d axis reluctance is higher than the q axis reluctance. This means that the q axis inductance L_q is higher than the d axis inductance L_d[Chandana,2002]. This brings saliency to this type of machine, where the saliency ratio is defined as:

$$\xi = \frac{L_q}{L_d} \tag{2.1}$$

The motor used in this project is a Sauer-Danfoss IPMSM. There is no data sheet for the motor. Some of the parameters, like the stator resistance R_s, number of poles p_b, L_d, L_q inductances, flux linkage of the permanent magnets Ψ_m are known from a previous project done using this motor. The data is presented in Table2.1 The mechanicals parameters, moment of inertia J, and the viscous friction coefficient B, need to be determined by measurements.

Parameter	Symbol	Value	Unit
Stator resistance	R_s	9.62	[mΩ]
D-axis inductance	L_d	28.7	[μH]
Q-axis inductance	L_q	47.2	[μH]
No. of pole pairs	p_b	6	-
PM flux linkage	Ψ_m	9.71	[mWb]

Table 2.1: *IPMSM electric parameters*

2.2 Mathematical model of the IPMSM

A mathematical model of the IPMSM is used in order to simulate the behavior of the machine in Matlab/Simulink. The model is expressed in the dq rotor reference frame, where the d axis is aligned with the rotor flux-linkage. The voltage stator-phase equations, in stator coordinates, of the IPMSM are as follows [Boldea,1999]:

$$\begin{aligned} u_a &= R_s \cdot i_a + \frac{d\Psi_a}{dt} \\ u_b &= R_s \cdot i_b + \frac{d\Psi_b}{dt} \\ u_c &= R_s \cdot i_c + \frac{d\Psi_c}{dt} \end{aligned} \tag{2.2}$$

where:

u_a, u_b and u_c are the stator phase voltages

R_s is the stator resistance

Ψ_a, Ψ_b and Ψ_c are the phase flux linkages

In order to have a simplified model of the machine the voltage equations are transformed from a 3 variable system to a 2 variable system using a coordinate system transformation from *abc* coordinates to *dq*. The *dq* system is linked to the rotor and is rotating at the synchronous speed of the stator. The transformation matrix is presented in Eq.2.3.

$$\begin{bmatrix} U_{s_d} \\ U_{s_q} \end{bmatrix} = \frac{2}{3} \begin{bmatrix} cos(\theta) & cos(\theta - \frac{2\pi}{3}) & cos(\theta - \frac{4\pi}{3}) \\ -sin(\theta) & -sin(\theta - \frac{2\pi}{3}) & -sin(\theta - \frac{4\pi}{3}) \end{bmatrix} \cdot \begin{bmatrix} u_a \\ u_b \\ u_c \end{bmatrix} \tag{2.3}$$

where

U_{s_d}, U_{s_q} are the d and q components of the stator voltage vector

θ is the angle between the stator fixed a axis and the rotor rotating d axis

The vector representation of the transformation is presented in Fig.2.3:

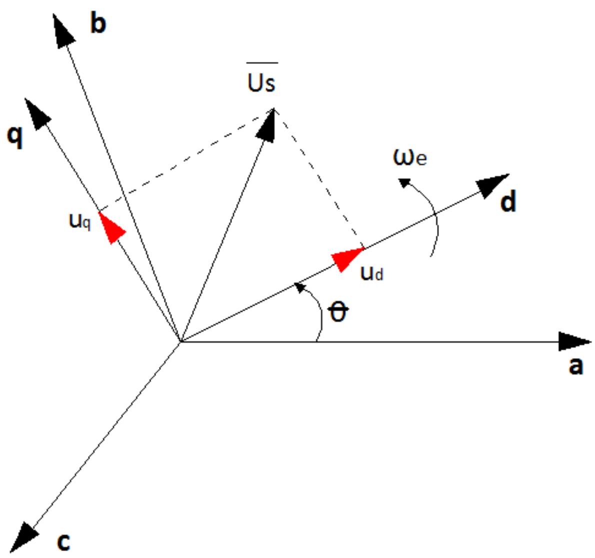

Figure 2.3: *Vector representation of the abc to dq frame transformation*

where

$\omega_e = \frac{d\theta}{dt}$ is the synchronous electrical speed

.

The angle θ is chosen so that the d axis is aligned with the flux linkage of the permanent magnets vector $\vec{\Psi_m}$. After the coordinate transformation is applied, the voltage equations for the IPMSM, expressed in the rotating dq reference frame are [Boldea,1999]:

$$U_{s_d} = Rs \cdot i_{s_d} + \frac{d\Psi_d}{dt} - \omega_e \cdot \Psi_q$$
$$U_{s_q} = Rs \cdot i_{s_q} + \frac{d\Psi_q}{dt} + \omega_e \cdot \Psi_d \tag{2.4}$$

where:

i_{s_d}, i_{s_q} are the dq stator currents

Ψ_d, Ψ_q are the dq flux linkages

The flux equations, in the dq reference frame are[Chandana,2002]:

$$\Psi_d = L_d \cdot i_d + \Psi_m$$
$$\Psi_q = L_q \cdot i_q \tag{2.5}$$

where:

Ψ_m is the flux linkage of the permanent magnets

The equivalent circuit representation of the voltage equations, in the dq reference frame is presented in Fig.2.4[Jahns,1986].

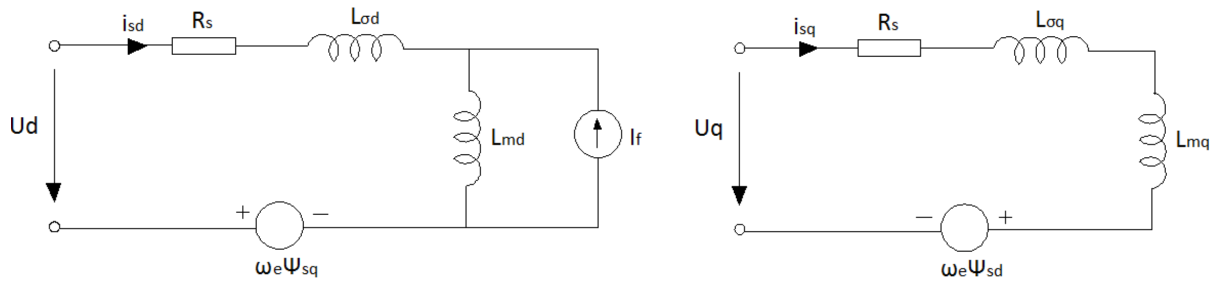

Figure 2.4: *Equivalent circuit representation of dq voltage equations fr an IPMSM*

where:

L_d=L_{σ_d}+L_{m_d}, L_{σ_d} and L_{m_d} are the d leakage and magnetizing inductance components

L_q=L_{σ_q}+L_{m_q}, L_{σ_q} and L_{m_q} are the q leakage and magnetizing inductance components

Ψ_m=$L_{m_d}I_f$, If is a fictive current source expressing the permanent magnets.

Torque equation. The produced electromagnetic torque of the IPMSM, expressed in the dq reference frame has the following expression[Boldea,1999]:

$$T_e = \frac{3}{2} p_b \cdot (\Psi_d \cdot i_{s_q} - \Psi_q \cdot i_{s_d}) \tag{2.6}$$

where:

p_b is the number of pole pairs

By substituting the flux equations from Eq.2.5, the torque equation becomes:

$$T_e = \frac{3}{2}p_b \cdot (\Psi_m \cdot i_{s_q}) + \frac{3}{2}p_b \cdot (L_d - L_q) \cdot i_{s_d} i_{s_q} \tag{2.7}$$

The electromagnetic torque has two components: the torque produced by the interaction of the stator current with the permanent magnet flux, and the so-called reluctance torque caused by the saliency of the motor, the difference between L_d and L_q inductances.

Mechanical equation. The mechanical equation of the machine is as follows:

$$T_e - T_l - T_d - B \cdot \omega_m = J \cdot \frac{d\omega_m}{dt} \tag{2.8}$$

where:

T_l is the load torque applied to the shaft of the motor

T_d is the dry friction torque

B is the viscous friction coefficient

$\omega_m = \frac{\omega_e}{p_b}$ is the shaft speed

J is the moment of inertia

2.3 Dynamic simulation of the IPMSM

The mathematical model of the IPMSM is implemented in Matlab/Simulink in order to check the behavior of the machine, at different speeds and torque levels. The Simulink model is also used in the overall control model, presented in the next chapter. The structure of the Simulink model is presented in Fig.2.5

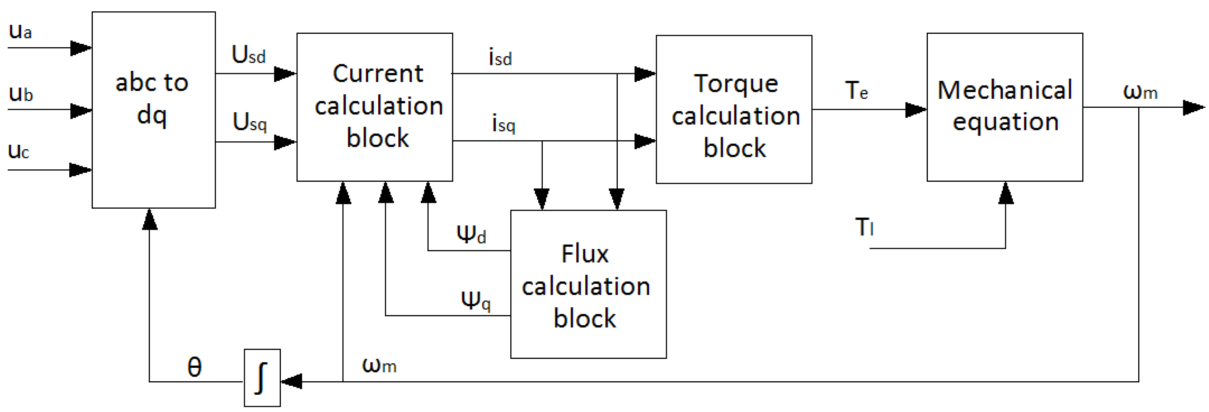

Figure 2.5: *Diagram representation of the simulation model for the IPMSM*

The inputs of the simulation model of the IPMSM are the phase voltages. The model outputs the shaft speed, and the stator currents. The applied phase voltages u_a, u_b and

u_c are transformed into the matching dq components, using the coordinate transformation presented in Eq.2.3. Using the flux equations presented in Eq.2.5 and also the stator voltage equations from Eq.2.4, the dq stator currents can be expressed as:

$$i_{s_d} = \frac{1}{L_d}(\int (U_{s_d} - R_s \cdot i_{s_d} + \omega_m p_b \cdot \Psi_q)dt - \Psi_m)$$
$$i_{s_q} = \frac{1}{L_q}\int (U_{s_q} - R_s \cdot i_{s_q} - \omega_m p_b \cdot \Psi_d)dt \tag{2.9}$$

The *Current calculation block* is presented in Fig.2.6.

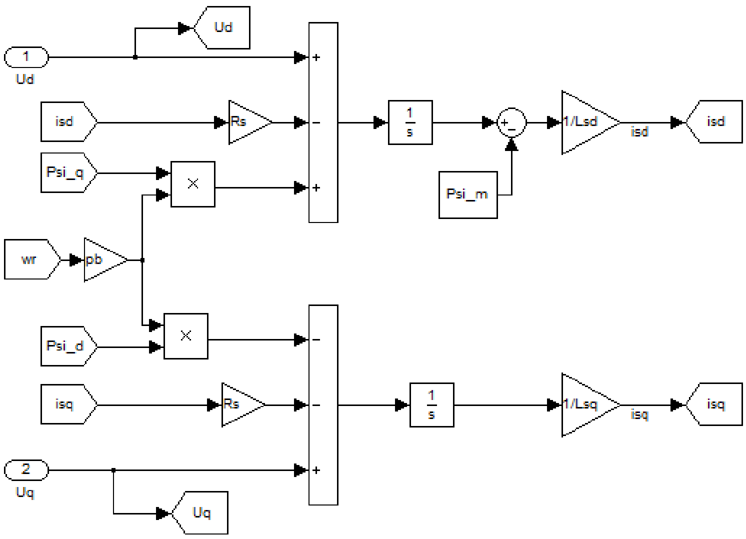

Figure 2.6: *Simulink model expressing the current calculation block*

The flux linkage calculation block is presented in Fig.2.7

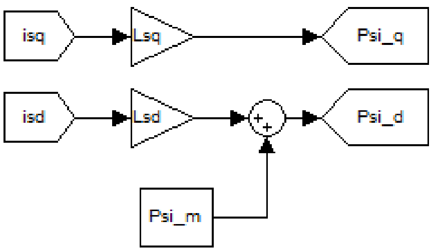

Figure 2.7: *Simulink model expressing the flux calculation block*

Having the currents known, the produced torque can be calculated according to Eq.2.7. If the mechanical equation presented in Eq.2.8 is also considered, the shaft speed can be calculated as in the following:

$$\omega_m = \frac{1}{J}\int (T_e - Tl - B \cdot \omega_m) \tag{2.10}$$

The Simulink model calculating the shaft speed, and also the angle θ is presented in Fig.2.8

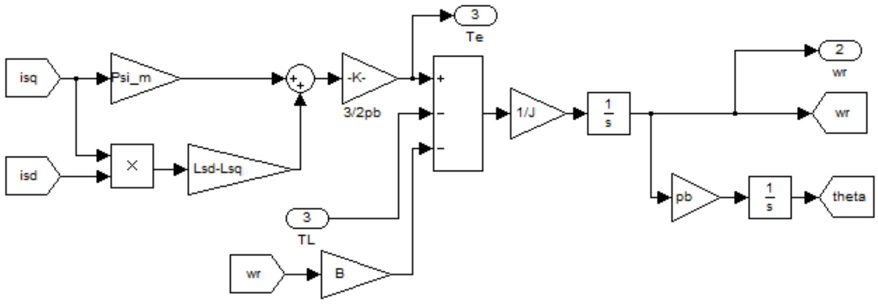

Figure 2.8: *Simulink model expressing the calculation of the shaft speed*

2.4 Motor mechanical parameters measurement

The electrical parameters of the Sauer-Danfoss IPMSM used in this project were presented in Table2.1. In order to run the dynamic simulation, the mechanical parameters need to be known also. The moment of inertia J, the dry friction torque T_d and the viscous friction coefficient B were measured using the setup presented in Fig.2.9

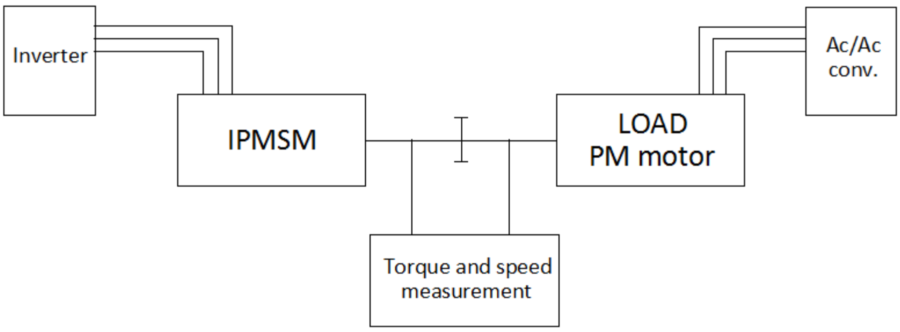

Figure 2.9: *Setup for determining the mechanical parameters of the IPMSM*

Two tests were done. In the first test, the viscous friction coefficient B, and the dry friction coefficient T_d, were determined. During this test the PM load machine was supplied with voltage, and thus used as a motor to drive the system. Starting from the mechanical equation of the PM machine:

$$T_e - T_l - B \cdot \omega_m - T_d = J \cdot \frac{d\omega_m}{dt} \tag{2.11}$$

if no load is applied T_l=0, and the steady state is considered $\frac{d\omega_m}{dt}$=0, the equation can be rewritten like in the following:

$$T_e - B \cdot \omega_m - T_d = 0$$

If two steady state-working points are known, (T_{e1}, ω_{m1}), and (T_{e2}, ω_{m2}), then B can be calculated according to:

$$B = \frac{T_e 2 - T_{e1}}{\omega_{m2} - \omega_{m1}} \tag{2.12}$$

Two measurements were done in steady-state, with no load. According to Eq2.12 the viscous coefficient was calculated. The results are presented in Table2.2. The dry friction

	Speed [rpm]	Speed [rad/s]	Torque [Nm]	Viscous friction coef [Nm*s/rad]
1	100	10.472	1	0.008488244
2	1000	104.72	1.8	

Table 2.2: *Steady state measurements*

torque is calculated from one of the measurements.

$$T_d = T_{e2} - B \cdot \omega_{m2} = 0.9099[Nm] \tag{2.13}$$

The second test was a run-out test, used to calculate the moment of inertia J. This time the IPMSM was used as a motor. The motor was run to 552[rpm], with no load applied, then the supply voltage was cut off, and the speed was recorded. The measured speed is presented in Fig.2.10

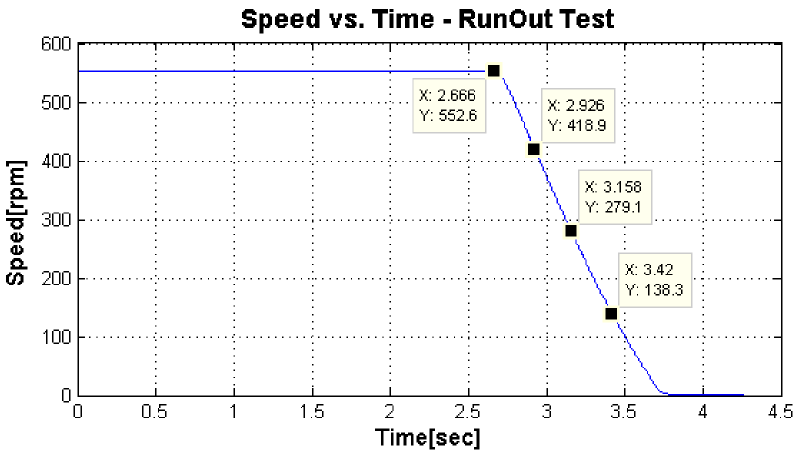

Figure 2.10: *Run-out test*

During the run-out test, after the supply voltage was cut off, 4 points from the speed curve are depicted to calculate the moment of inertia, like shown in Fig.2.10. These points are the starting point(when the voltage was cut off), and 3 other points, that divide the time interval from the start of the procedure until full stop in 4 equal parts[PED8].

Taking into consideration the mechanical equation from Eq.2.11, when no load is applied, J can be calculated as follows:

$$J = \frac{T_d + B \cdot \omega_m}{-\frac{d\omega_m}{dt}} \tag{2.14}$$

The measured data and the results are presented in Table2.3

	Time [sec]	Speed [rpm]	Speed [rad/s]	Time difference [sec]	Speed difference [rad/s]	J [kg*m2]	J(mean) [kg*m2]
Start point	2.666	552.6	57.868272				0.02017768
Point 1	2.926	418.9	43.867208	0.26	-14.001064	0.023821	
Point 2	3.158	279.1	29.227352	0.232	-14.639856	0.018356	
Point 3	3.42	138.3	14.482776	0.262	-14.744576	0.018356	

Table 2.3: *Table with the measured data for calculating the moment of inertia J*

The calculated mechanical parameters of the IPMSM are:

$J = 20.17 \cdot 10^{-3}\ [kg \cdot m^2]$

B=0.0085 $[Nm \cdot \frac{sec}{rad}]$

Td=0.909 [Nm]

2.5 Simulation results

There is no information regarding the nominal working point of the IPMSM. In order to check the behaviour of the machine, the IPMSM model employed was tested at different speeds with different load torques. The electrical parameters of the machine used for the simulation are the same as in Table2.1. For simplicity, from the mechanical parameters only the moment of inertia J was used.

No load test at 1500rpm

First the IPMSM model was tested at no load. The speed was set to 1500rpm. The phase voltages of the motor are plotted in Fig.2.11. As shown in the plot, the amplitude of the stator phase voltage, at no load, is U=9.15V.

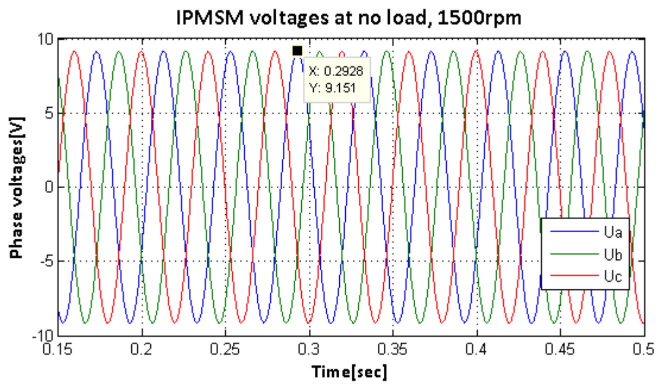

Figure 2.11: *Phase voltage at 1500rpm, with no load*

Test at 10Nm and 15 Nm load at a speed of 1000rpm

For the second test the speed of the motor was set to 1000rpm. The motor was loaded with 10Nm and 15Nm. The phase voltages and phase currents for the two working points are plotted in Fig.2.12 and Fig.2.13

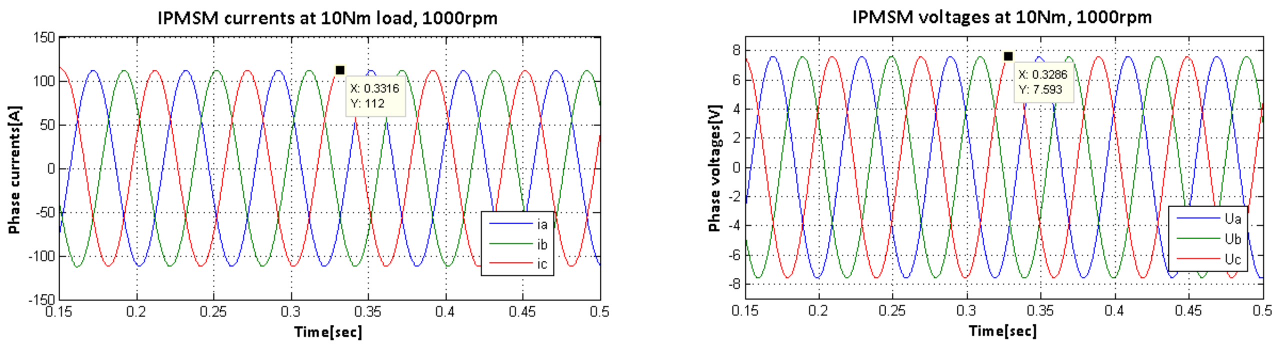

Figure 2.12: *Phase voltages and phase currents at 1000rpm, with 10Nm load*

The amplitude of the phase voltage at 10Nm and 1000rpm is U=7.6V. The amplitude of the phase current is I=112A. For the same speed when a load of 15Nm is applied, the phase current increases to I=164.4A. The change in phase voltage is very small, from U=7.6V to U=8.5V.

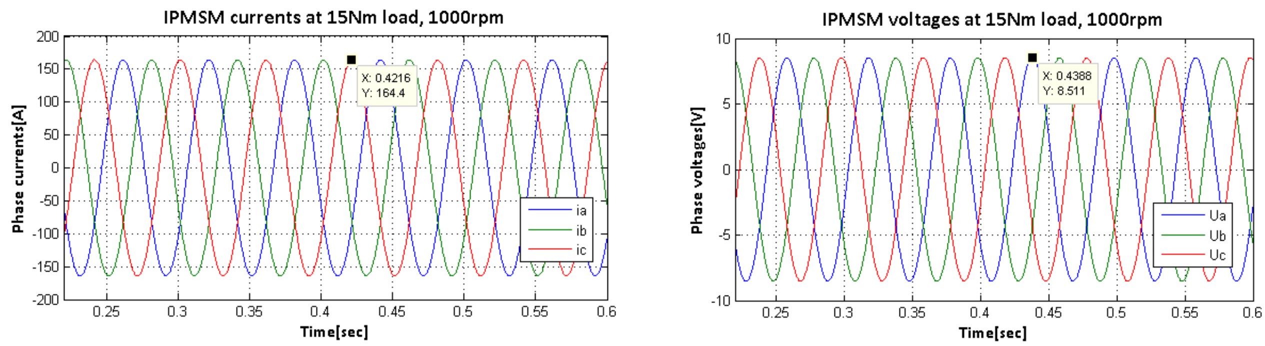

Figure 2.13: *Phase voltages and phase currents at 1000rpm, with 15Nm load*

Test at 10Nm and 15 Nm load at a speed of 1500rpm

A final test was done, at the same values for load torque as the previous test, but for an elevated speed, n=1500rpm. As shown in Fig.2.13, the phase current at 1500 rpm and 10Nm is I=111A, which is almost the same with the current level for the same torque but at 1000rpm. Due to the higher speed, the phase voltage, compared with the voltage at 1000rpm, is higher, U=10.88V.

When the load was increased to 15 Nm, at 1500rpm, Fig.2.14, the phase currents also increased, as expected to I=164.4. Taking a look at the phase voltage, it increases from U=10.88V at 10Nm, to U=12.06V.

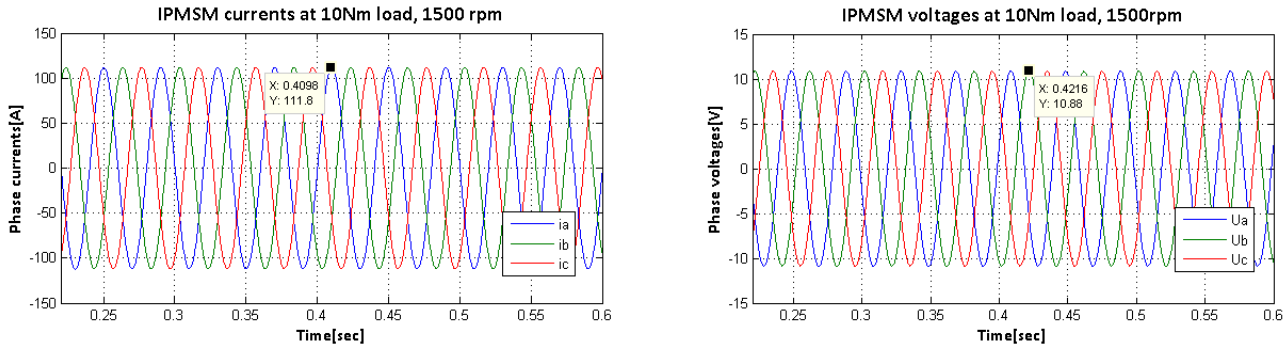

Figure 2.14: *Phase voltages and phase currents at 1500rpm, with 10Nm load*

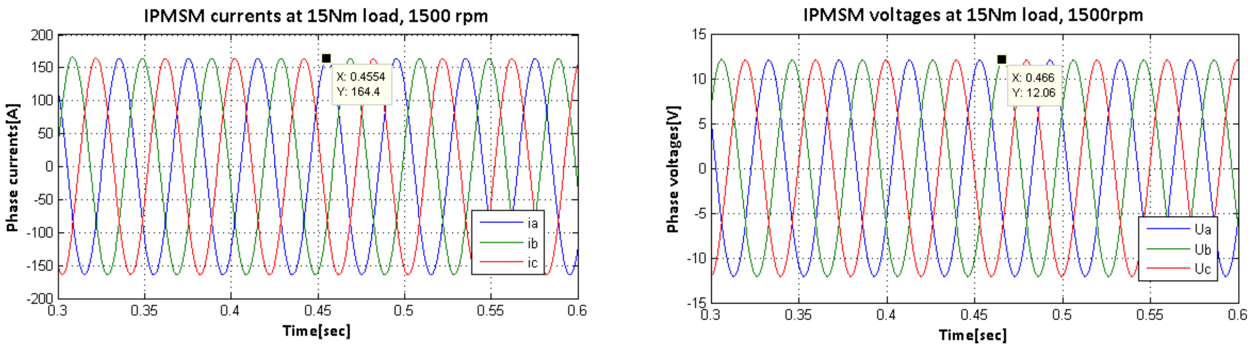

Figure 2.15: *Phase voltages and phase currents at 1500rpm, with 15Nm load*

Considering the implementation of the control designed in the next chapter in a real-life system, it shoud be mentioned that the IPMSM is supplied with a 3-phased inverter, having a DC-link of 24V. Using a space vector modulation technique the maximum voltage that can be extracted is around 13.8 V in phase amplitude. From the tests presented above, at 1500rpm, with a load of 15Nm, the phase voltage U=12V, is very close to the maximum available voltage from the inverter.

As a conclusion to the tests performed, if the motor is run at a speed of 1500rpm, the motor can be loaded up to 15Nm, before reaching the maximum available voltage. It is reasonable to assume that the working nominal point of the motor is between(1000rpm-1500rpm), at a load between (10-15Nm). Depending on the current limitation, the load may be increased above 15 Nm, at lower speeds.

In this chapter the main characteristics of an interior PMSM were presented. The mathematical model, in the *dq* reference frame was derived, and used in a Matlab/Simulink simulation file for implementation. Using the developed model several tests were done, at different speeds and different loads to investigate the working point of the machine.

3
Control of IPMSM

This chapter presents the implementation of the Field Oriented Control(FOC), together with the Field Weakening(FW) algorithm. Starting from the general topology of FOC, the Maximum Torque per Ampere(MTPA) control is presented, and also the tuning of the PI parameters. Next the FW algorithm chosen is presented. In the end the overall simulation model is presented, together with the simulation results.

3.1 Introduction

The main principle in any machine control is to keep the desired speed of the machine constant, subject to any changes in the load torque applied. In order to have the desired speed, the produced torque of the machine has to be controlled. Taking a look at the mathematical equation of the produced torque of the IPMSM,

$$T_e = \frac{3}{2}p_b \cdot (\Psi_m \cdot i_{s_q}) + \frac{3}{2}p_b \cdot (L_d - L_q) \cdot i_{s_q} i_{s_q}$$

the torque can be fully determined by controlling the i_{s_q} and i_{s_d} current components(considering that the inductances L_d and L_q are constant). The IPMSM is an ordinary AC machine, which has distributed windings in the stator slots, that produce a rotating field when supplied with a 3-phased balanced voltage system. So the main types of motor control algorithms, used to drive an induction machine can be applied also to the permanent magnet machine. The three main types of motor control are[PED8]:

U/f Control, in open loop

Field Oriented Control(FOC), in closed loop

Direct Torque Control(DTC), in closed loop

The ***U/f*** control is used in simple applications like pumps and fans, where there is no need for a high performance drive. The main features of this kind of control are: the controlled variables are the voltage and the frequency, the motor is fed with constant voltage/frequency ratio (the stator flux is constant), it is an open loop control, there is no need for a feedback. The main advantage of this type of control is its low price. The drawbacks are that the torque is not controlled(the level of the torque is set by the load), and the status of the rotor is ignored, no feedback of the speed of the shaft or of the currents is used.[ABB]

The ***FOC*** is the best solution for low speed applications like cranes and high performance drives.[PED8] This type of control is a closed loop control. It uses the speed of the shaft, provided by an encoder, as a feedback in the control strategy. Besides this speed loop, there is also a current loop that controls the electro-magnetic torque produced by the machine. It is for this reason that the FOC is also called an indirect control(the torque is indirectly controlled through the currents). The main advantages of this type of control are: it has an accurate speed control, it has a good torque response, and it achieves full torque at zero speed.[ABB] The main disadvantages of the FOC are that it has a high cost, and also in order to drive the machine, a modulation technique must be used to control the inverter.

The ***DTC*** achieves field orientation without any speed feedback, using advanced machine theory to calculate the motor torque directly, and without using modulation. The controlled variables are the motor torque and the magnetizing flux linkage.[ABB] This is done by controlling the power switches of the inverter directly, by selecting an appropriate voltage vector from a predefined switching table. The advantage of this type of control is that the torque response is faster than when using classical FOC. The disadvantage of this control is that when it is applied on a PMSM, the rotor position also has to be known[PED8]

This project deals with the control of an Interior PMSM. The control strategy chosen should be capable of good and fast torque response, and also be capable of Field Weakening, to increase the speed of the machine above the rated synchronous speed. The control strategy that suits best is Indirect Field Oriented Control. Thus FOC is chosen to drive the permanent magnet motor.

3.2 Field Oriented Control

The FOC is an indirect closed loop control method. The speed of motor needs to be measured, and fed as a feedback, in order to perform this algorithm. The torque produced by the permanent magnet motor is controlled indirectly, by controlling the stator current i_s. The control algorithm is expressed in the rotating dq rotor reference frame, that has its d axis aligned with the flux-linkage of the permanent magnet vector $\vec{\Psi_m}$. A phasor diagram representing the dq frame chosen is presented in Fig.3.1

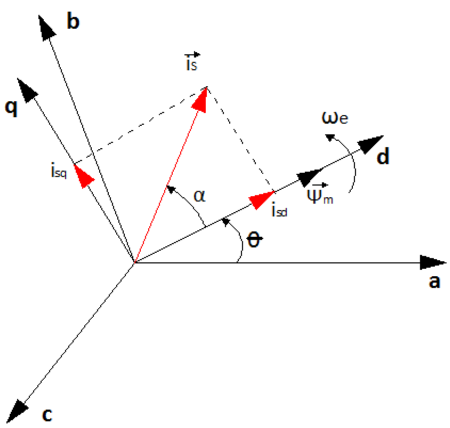

Figure 3.1: *Phasor diagram illustrating the dq control reference frame*

where:

α is the torque angle

$i_s = i_{s_d} + j i_{s_q}$

In order to perform this control, a modulation technique, for controlling the switches of the inverter has to be utilized also. Space Vector Modulation(SVM) is chosen as a control method for the inverter. The overall control structure is presented in Fig.3.2

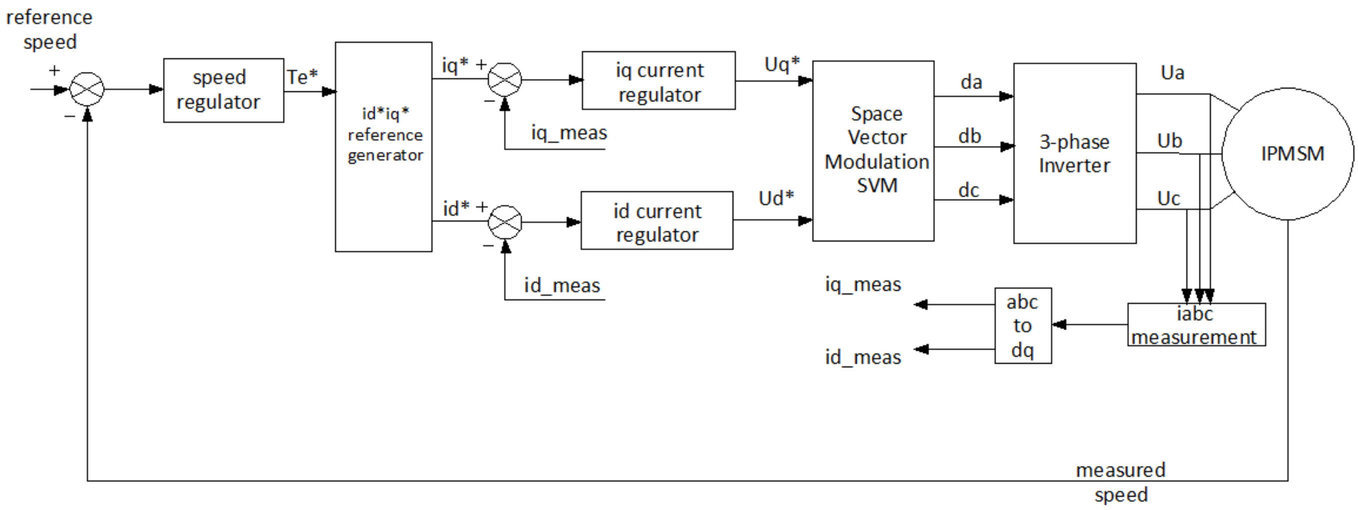

Figure 3.2: *Field Oriented Control - general structure*

There are 2 control loops: the speed loop, that controls the speed of the motor, and the current loop(for both i_{s_d} and i_{s_q} currents) that controls the torque of the motor. In order to assume that the current control loop has no influence on the speed loop, the bandwidth of the current loop should be at least 6-8 times higher than the bandwidth of the speed loop.[PED8].

The desired speed of the motor is the input of the control system, like shown in Fig.3.2. Using the measured speed, the error between the reference speed and the actual speed of the motor is fed to a speed regulator. The output of this regulator is a torque command T_e*. From this torque command the reference currents, $i_{s_d}*$ and $i_{s_d}*$, are depicted, based on one of this control strategies[Chandana,2002]:

- Constant torque angle control($\alpha = \frac{\pi}{2}$) (CTA)
- Maximum torque per ampere control (MTPAC)
- Unity power factor control (UPFC)
- Constant stator flux control (CSTC)

From the strategies presented above, the control chosen is *Maximum torque per ampere*(MTPA).

The error between the reference dq currents, chosen by the MTPA algorithm, and the measured dq currents is fed to the current regulators. The output of the current regulators are the corresponding dq reference stator voltages. Based on these stator voltages, space vector modulation is used to control the switches of the inverter.

The regulators used in the control algorithm are chosen to be Proportional-Integrator(PI) regulators. The FOC algorithm is expressed in the rotor dq frame, in which the currents and voltages are considered as constant values, so the PI controllers can eliminate the steady-state error.

3.3 Maximum torque per ampere control

The MTPA control strategy assures that for a required torque level the minimum stator current magnitude is applied. By doing this the copper losses are minimized, and the overall efficiency of the motor can be increased.[Chandana,2002][Jahns,1986]

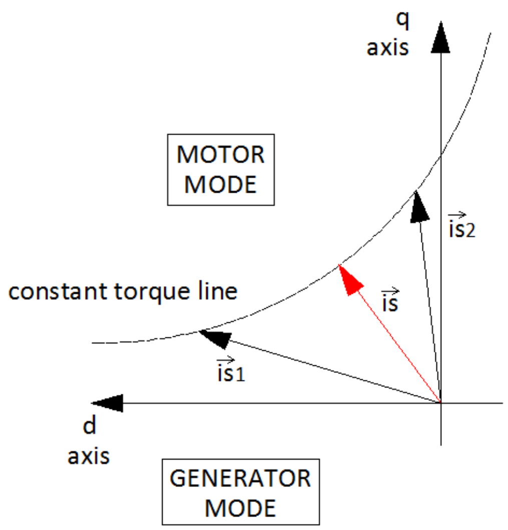

Figure 3.3: *Vector representation of the minimum stator current vector at a given torque level for an IPMSM[Jahns,1986]*

Like presented in Fig.3.3, at a given torque, from the multiple possibilities of stator current vectors(ex.$\vec{i_{s1}}, \vec{i_{s2}}$) that can produce the desired torque level, $\vec{i_s}$(red) is the one that is minimum. All the points given by the intersection of the minimum current vectors and the corresponding torque levels give the MTPA curve.

The starting point in obtaining the MTPA curve for the IPMSM is the electro-magnetic torque equation of the machine.

$$T_e = \frac{3}{2}p_b \cdot (\Psi_m \cdot i_{s_q}) + \frac{3}{2}p_b \cdot (L_d - L_q) \cdot i_{s_d} i_{s_q}$$

Besides this equation one more constraint needs to be added, that is the limitation of the stator current, due to the physical current limitation of the inverter.

$$I_{s_{max}}^2 = i_{s_d}^2 + i_{s_q}^2 \tag{3.1}$$

where:

$I_{s_{max}}$ is the maximum amplitude of the current which is supported by the inverter

If i_{s_q} is depicted from Eq.3.1 and substituted into the torque equation the following expression is obtained

$$T_e = \frac{3}{2}p_b \cdot (\Psi_m \sqrt{I_{s_{max}}^2 - i_{s_d}^2}) + \frac{3}{2}p_b \cdot (L_d - L_q) i_{s_d} \sqrt{I_{s_{max}}^2 - i_{s_d}^2} \tag{3.2}$$

In order to find the minimum i_{s_d} that satisfies the torque equation, the torque T_e has to be derivated with respect to i_{s_d}. The expression of the torque variation with respect to the d axis stator current is:

$$\frac{dT_e}{di_{s_d}} = \frac{3}{2}p_b \cdot \frac{-i_{s_d}\Psi_m + (L_d - L_q)(I_{s_{max}} - 2i_{s_d}^2)}{\sqrt{I_{s_{max}}^2 - i_{s_d}^2}} \tag{3.3}$$

This leads to :

$$2i_{s_d}^2 + \frac{\Psi_m}{L_d - L_q} \cdot i_{s_d} - I_{s_{max}}^2 = 0 \tag{3.4}$$

From this equation the minimum i_{s_d} current that satisfies the torque equation is found.

$$i_{s_d} = \frac{-\Psi_m + \sqrt{\Psi_m^2 + 8(L_d - L_q)^2 I_{s_{max}}^2}}{4(L_d - L_q)} \text{[Jonas,2006][Boldea,1999]} \tag{3.5}$$

Finally the set of equations that give the MTPA curve of an IPMSM, and also the relationship between the reference torque and the corresponding stator currents, i_{s_d}*=f(T_e*) and i_{s_q}*=f(T_e*) are:

$$\begin{aligned} T_e &= \frac{3}{2}p_b \cdot (\Psi_m \cdot i_{s_q}) + \frac{3}{2}p_b \cdot (L_d - L_q) \cdot i_{s_d} i_{s_q} \\ i_{s_d} &= \frac{-\Psi_m + \sqrt{\Psi_m^2 + 8(L_d - L_q)^2 I_{s_{max}}^2}}{4(L_d - L_q)} \\ i_{s_q} &= \sqrt{I_{s_{max}}^2 - i_{s_d}^2} \end{aligned} \tag{3.6}$$

As presented in Eq.3.6 the MTPA curve is dependent of the machine parameters: the flux linkage of the permanent magnets, and the d and q axis inductances. A Matlab program[Boldea,1999] was used to derive the MTPA curve for the IPMSM used in this project. The motor parameters are the ones presented in Chapter2. The maximum current magnitude is set to $I_{s_{max}}$=300A.

L_d=28.7[μH],L_q=47.2[μH], Ψ_m=9.71[mWb]

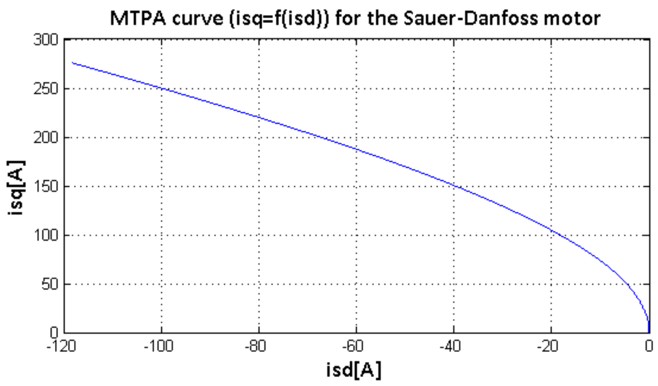

Figure 3.4: *MTPA curve for the Sauer-Danfoss motor used in this project*

The motor parameters,Ψ_m, L_d and L_q that determine the shape of the MTPA curve are considered constant. The variation of the Ld,Lq inductances due to the current variation, or saturation is not considered. This may influence the performance of the MTPA control in the real-system application, due to the actual variation of the motor parameters during the running of the motor. In order to see the influence of the motor parameters on the MTPA curve, the L_d and L_q inductances were varied and the MTPA curves were plotted. The variation of the MTPA curve with the variation of the L_d inductance is presented in Fig.3.5

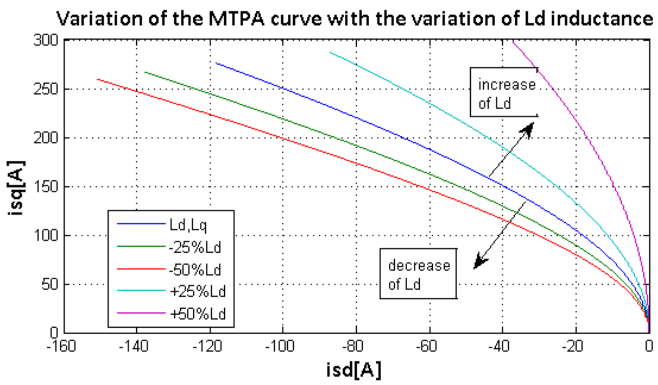

Figure 3.5: *MTPA curve for the Sauer-Danfoss motor with varying Ld inductance*

If the L_d inductance is decreasing the slope of the MTPA curve is also decreasing. Translated into d and q axis currents it means that for a given torque, the i_{s_d} (flux current) is increased, and the i_{s_q}(torque current) is decreased. On the other hand if the variation of the L_d inductance is positive the slope of the curve is increasing. This will give a smaller i_{s_d} current for the same torque but a higher i_{s_q}. As seen in Fig.3.5 The MTPA curve is more sensitive to an increase of the L_d inductance.

Taking a look at the variation of the MTPA curve with the variation of the L_q inductance from Fig.3.6, if the L_q inductance is decreasing, the slope of the curve is increasing. Translated into dq currents it means that for the same torque the i_{s_q} current is increased while the i_{s_d} current is decreased. When the variation of the L_q inductance is positive, the slope of the curve is decreasing. So for the same torque, the i_{s_d} current is increased, while i_{s_q}

is decreased. As an observation the variation of the MTPA curve is larger with the decrease of the L_q inductance.

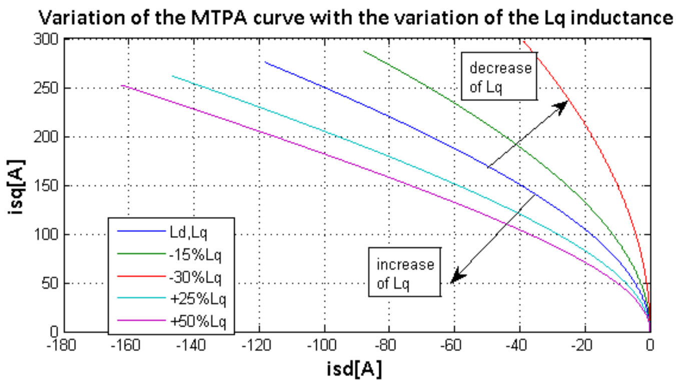

Figure 3.6: *MTPA curve for the Sauer-Danfoss motor with varying Lq inductance*

If the MTPA curve is known, using the expression of the electro-magnetic torque of the machine, the relations i_{s_d}*=f(T_e*) and i_{s_q}*=f(T_e*) needed for the FOC control can be determined. The variation of the torque, correspondent to the MTPA curve is presented in Fig.3.7

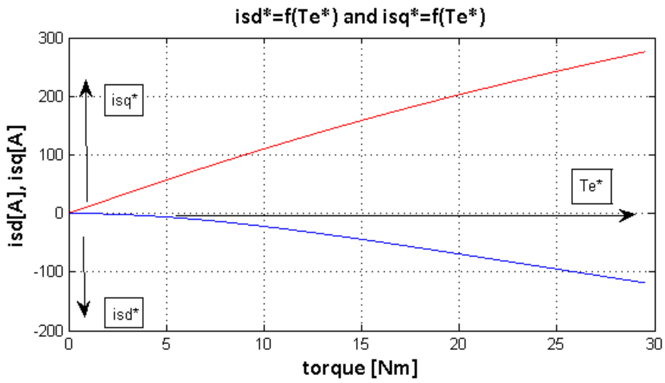

Figure 3.7: *Generation of the reference isd* and isq* currents(MTPA curve) from the torque reference*

This information regarding the reference currents from the reference torque command, is used in the FOC simulation model as a feed-forward control. The data i_{s_d}*=f(T_e*) and i_{s_q}*=f(T_e*) is stored in look-up tables. The Matlab/Simulink model is presented in Fig.3.8

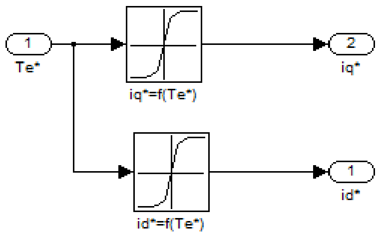

Figure 3.8: *Simulin model of the feed-forward control using look-up tables*

3.4 Tuning of the PI current controllers

The 2 inner current loops(for i_{s_d} and i_{s_q}) are much faster that the speed loop. Based on this, the PI current controllers are tuned first. The diagram representation of the PI current controllers structure is presented in Fig.3.9

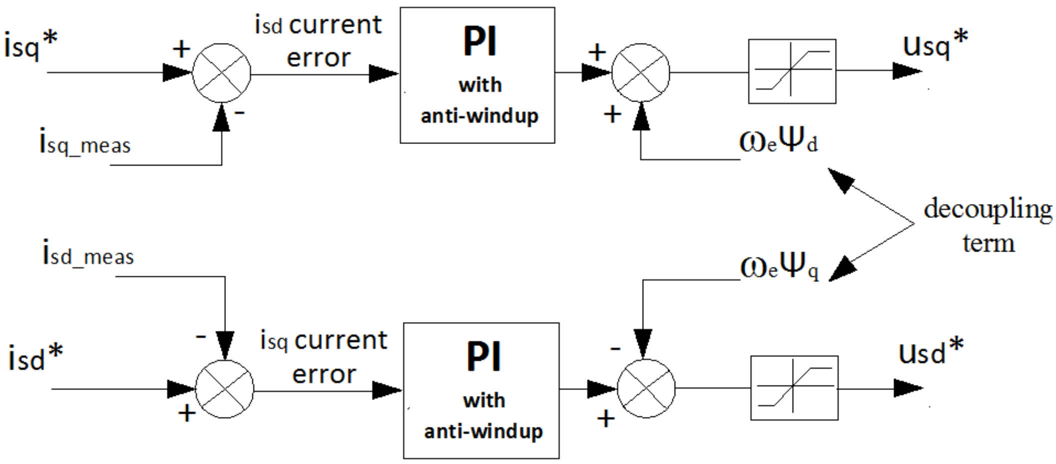

Figure 3.9: *Structure of the PI current controllers*

The error between the dq reference currents and the measured ones is fed to the PI controllers. The output of the PI controllers is the corresponding d and q voltages. The output of the PI controllers is limited, so a PI configuration with anti-windup is used. A decoupling term is used on both current loops in order to control the i_{s_d} and i_{s_q} individually. The decoupling term, the back-emf $\omega\Psi$, is depicted from the 2 voltage equations of the IPMSM.

$$U_{s_d} = R_s \cdot i_{s_d} + \frac{d\Psi_d}{dt} - \omega_e \cdot \Psi_q$$

$$U_{s_q} = R_s \cdot i_{s_q} + \frac{d\Psi_q}{dt} + \omega_e \cdot \Psi_d$$

The 2 voltage equations are coupled by the back-emf term. By subtracting this term in the 2 current loops, the 2 currents i_{s_d} and i_{s_q} can be controlled independently. This also simplifies the transfer function of the IPMSM in the two current loops. The voltage equations expressed in the s plane are:

$$U_{s_d}(s) = R_s i_{s_d}(s) + s \cdot L_d \cdot i_{s_d}(s) \tag{3.7}$$

$$U_{s_q}(s) = R_s i_{s_q}(s) + s \cdot L_q \cdot i_{s_q}(s) \tag{3.8}$$

This gives the following transfer function of the IPMSM for the d and q current loop:

$$P_d(s) = \frac{1}{s \cdot L_d + R_s} = \frac{1}{R_s(s \cdot T_{sd} + 1)} \tag{3.9}$$

$$P_q(s) = \frac{1}{s \cdot L_q + R_s} = \frac{1}{R_s(s \cdot T_{sq} + 1)} \tag{3.10}$$

where:

T_{sd}=$\frac{L_d}{R_s}$ is the d electrical time constant

T_{sq}=$\frac{L_q}{R_s}$ is the q electrical time constant

3.4.1 Tuning the i_{s_q} PI controller

The i_{s_q} current loop is presented in Fig.3.10[PED9]

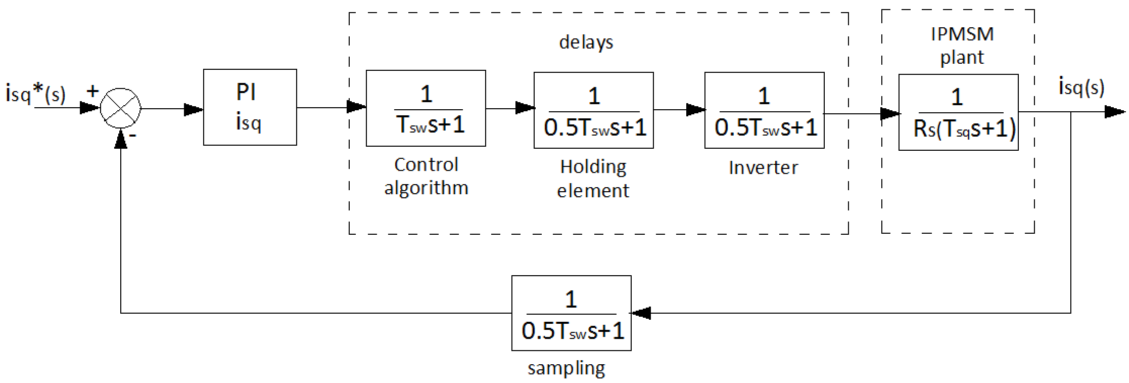

Figure 3.10: *Design of the i_{s_q} current loop*

The tuning of the PI controller is done in the continuous ’s’ domain. Delays have been introduced, due to the delays in the real-life discrete system, that the controller is going to be applied to. These delays are[PED9]:

- the delay due to the digital calculation(control algorithm); the delay is introduced by a first order transfer function having the time constant T_{sw}=$\frac{1}{f_{sw}}$=0.2ms(f_{sw}=5kHz is the switching and also sampling frequency used in the real-time application);

- the delay due to the sample and hold element(sampling); the delay is introduced by a first order transfer function that has the time constant equal to 0.5*T_{sw}=0.1ms;

- the delay introduced by the modulation technique and the inverter; the delay is introduced by a first order transfer function that has the time constant equal to 0.5*T_{sw}=0.1ms;

The transfer function of the PI controller is given by[Kazmierkowski]:

$$PI_q = k_{p_q} \frac{1 + \tau_q \cdot s}{\tau_q \cdot s} \tag{3.11}$$

The i_{s_q} current loop can be redrawn to have a unity feedback[Ogata,1997]. The control structure is represented in Fig.3.11.

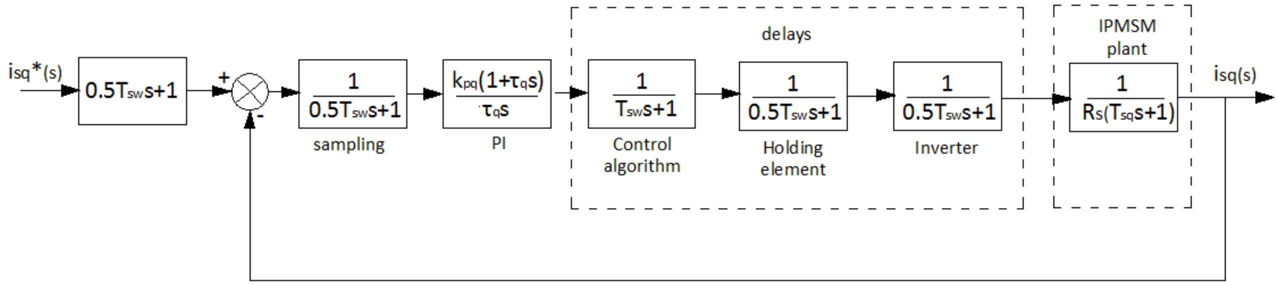

Figure 3.11: *Design of the i_{s_q} current loop with unity feedback*

The open loop transfer function of the i_{s_q} loop has the following expression:

$$G_{ol_q} = \frac{k_{p_q}(1 + \tau_q \cdot s)}{\tau_q \cdot s} \cdot \frac{1}{0.5T_{sw}s + 1} \cdot \frac{1}{T_{sw}s + 1} \cdot \frac{1}{0.5T_{sw}s + 1} \cdot \frac{1}{0.5T_{sw}s + 1} \cdot \frac{1}{R_s(s \cdot T_{sq} + 1)} \tag{3.12}$$

The root-locus of the open loop transfer function, for the q current loop is presented in Fig.

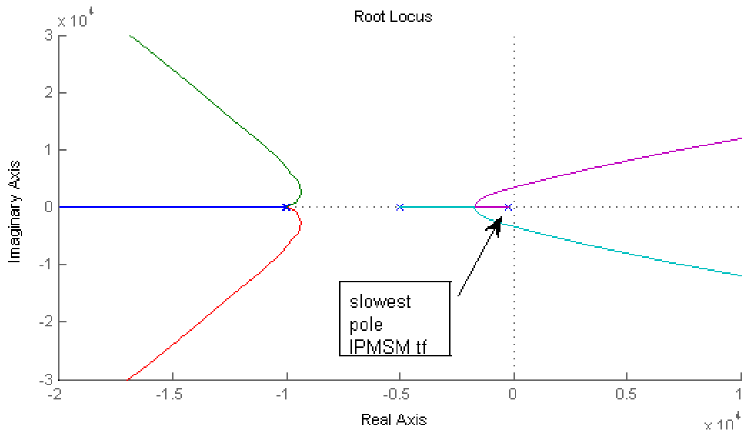

Figure 3.12: *Root locus for the q current open loop transfer function*

The slowest pole is the one of the IPMSM transfer function. Therefore the zero of the PI transfer function is set to cancel-out this pole. This gives:

$$\tau_q = \frac{L_q}{R_s} = T_{sq} = 0.0049 \tag{3.13}$$

In order to find out the gain of the PI controller, all the first order transfer functions that introduce delays are approximated by one transfer function that has the time constant equal to:

$$T_{s_i} = 3 \cdot 0.5T_{sw} + T_{sw} = 4T_{sw} = 0.5ms \tag{3.14}$$

The equivalent open loop transfer function, taking account of the canceling-out of the pole of the IPMSM transfer function, and also of the approximated time constant of the delays is as follows:

$$G_{ol_q} = \frac{k_{p_q}}{\tau_q \cdot s} \cdot \frac{1}{R_s(T_{s_i}s + 1)} \tag{3.15}$$

The *Optimal Modulus*(OM) design criterion is used in order to calculate the gain of the PI q current controller, where the damping factor is chosen $\xi = \frac{\sqrt{2}}{2}$. Based on the OM criterion, the generic open-loop transfer function for a second order system, with the damping factor $\xi = \frac{\sqrt{2}}{2}$ has the following expression[PED9]:

$$G = \frac{1}{2\xi s(1 + \xi s)} \tag{3.16}$$

Comparing this generic expression of the second order transfer function with the open loop transfer function of the i_{s_q} current from Eq.3.15, the gain of the PI controller can be found.

$$\frac{k_{p_q}}{R_s \cdot \tau_q} = \frac{1}{2T_{s_i}} \Rightarrow k_{p_q} = R_s \frac{\tau_q}{2T_{s_i}} = 0.0471 \tag{3.17}$$

The transfer function of the PI controller has then the following expression:

$$PI_q = \frac{0.0471(1 + 0.0049s)}{0.0049s} = 0.0471 + \frac{9.6122}{s} \tag{3.18}$$

The Bode diagram of the open loop system is plotted in Fig.3.13

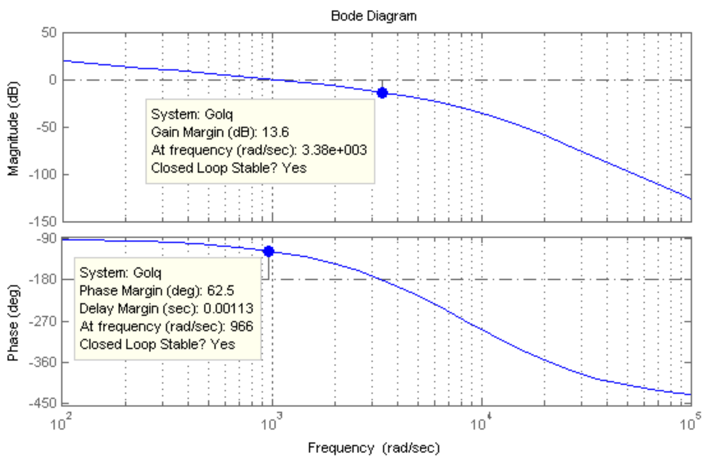

Figure 3.13: *Bode plot for the i_{s_q} loop*

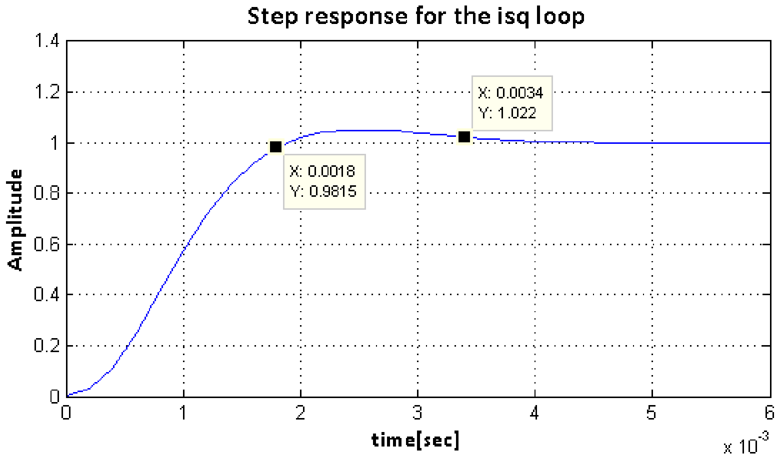

Figure 3.14: *Step response for the i_{s_q} loop*

As shown in Fig.3.13 the i_{s_q} closed loop system is stable. The gain margin is GM=13.6db, and the phase margin is PM=62.5deg. The step response of the closed loop system is presented in Fig.3.14.

The step response is characterized by the following parameters:

- rise time t=1.8ms
- settling time t=3.5ms
- maximum overshoot Mp=5%

In the following an equivalent time constant for the i_{s_q} loop is derived. The reason for doing this is that this time constant, viewed as a delay, will be used in the tuning of the speed controller.[PED9] Taking account of the transfer function of the PI controller the close loop transfer function has the following configuration:

$$G_{cl_q} = \frac{1}{2T_{s_i}^2 s^2 + 2T_{s_i} s + 1} \tag{3.19}$$

The q current loop can be expressed now like in Fig.3.15

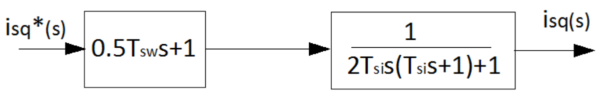

Figure 3.15: *i_{s_q} current loop*

If the transfer function $0.5T_{sw} + 1$ is approximated like

$$0.5T_{sw}s + 1 \approx \frac{1}{1 - 0.5T_{sw}s} [\text{PED9}] \tag{3.20}$$

then the q current closed loop transfer function becomes:

$$\frac{i_{s_q}*}{i_{s_q}} = \frac{1}{1 - 0.5T_{sw}s} \cdot \frac{1}{2T_{s_i}^2 s^2 + 2T_{s_i}s + 1} \tag{3.21}$$

If the second order term is neglected, then an equivalent time constant for the i_{s_q} current loop can be estimated. This time constant is equal to:

$$T_i q = 2T_{s_i} - 0.5T_{sw} = 0.9ms \tag{3.22}$$

3.4.2 Tuning the i_{s_d} PI controller

The i_{s_d} current loop is presented in Fig.3.16

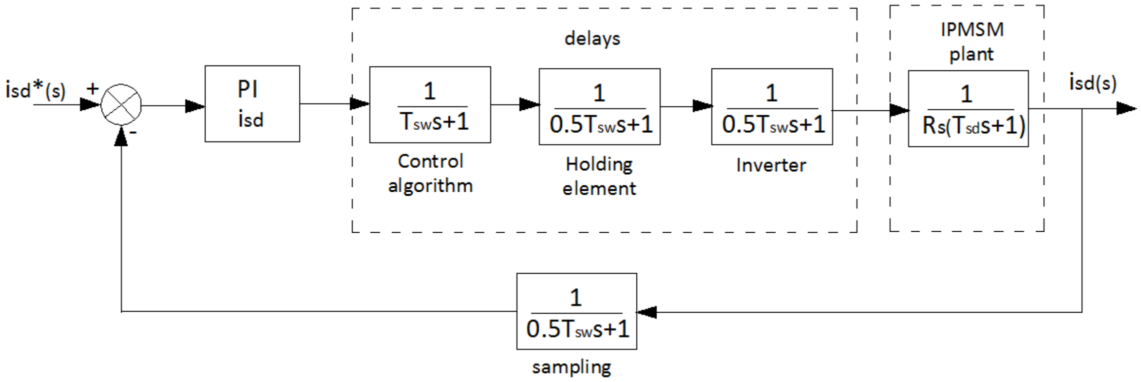

Figure 3.16: *Design of the i_{s_d} current loop*

The tuning of the d current loop is designed the same as the q current loop, in the continuos 's' domain. Therefore delays have been introduced, due to the delays in a real-life system. These delays are the same as for the i_{s_q} current loop. The only difference from the q current loop is the transfer function of the IPMSM, which is different due to the difference in the L_d, L_q inductances.

The transfer function of the PI, d loop, controller is:

$$PI_d = k_{p_d} \frac{1 + \tau_d \cdot s}{\tau_d \cdot s} \tag{3.23}$$

In order to have a unity feedback, the d current loop can be redrawn like in Fig.3.17

Based on the diagram in Fig.3.17, the open loop transfer function of the i_{s_d} current loop is:

$$G_{ol_d} = \frac{k_{p_d}(1 + \tau_d \cdot s)}{\tau_d \cdot s} \cdot \frac{1}{0.5T_{sw}s + 1} \cdot \frac{1}{T_{sw}s + 1} \cdot \frac{1}{0.5T_{sw}s + 1} \cdot \frac{1}{0.5T_{sw}s + 1} \cdot \frac{1}{R_s(s \cdot T_{sd} + 1)} \tag{3.24}$$

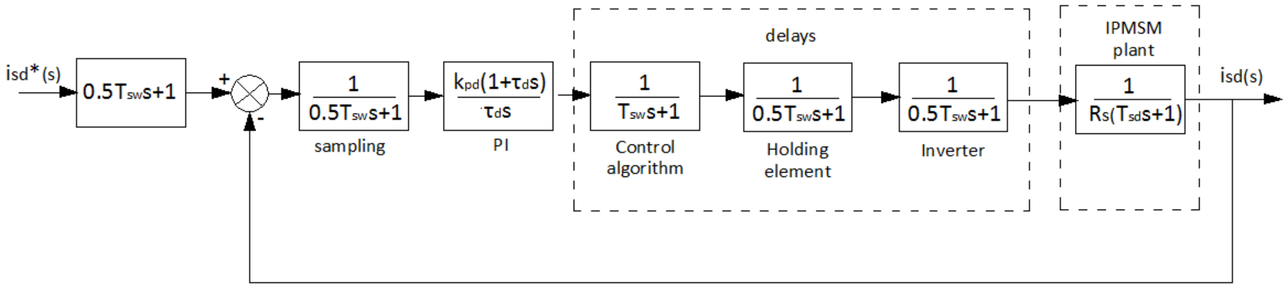

Figure 3.17: *Design of the i_{s_d} current loop with unity feedback*

The root-locus of the d current open loop is presented in Fig.3.18

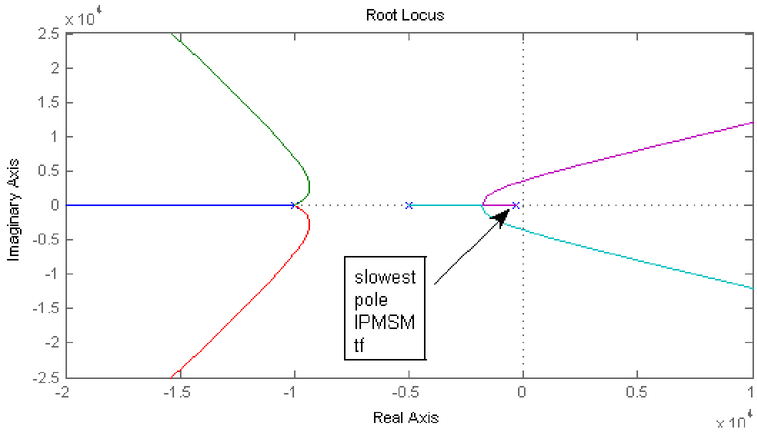

Figure 3.18: *Root locus for the d current open loop transfer function*

From the root-locus plot it can be seen that the slowest pole is situated at -336 on the real axis. Therefore the zero of the PI transfer function is chosen to cancel-out thi pole. This gives that:

$$\tau_d = \frac{L_d}{R_s} = T_{sd} = 0.003 \tag{3.25}$$

In order to find the gain of the PI, d current, transfer function, an equivalent time constant is calculated based on all the time constants of the delays introduced. The delays are the same as for the q current loop, so the equivalent time constant has the same value as for the q current loop.

$$T_{s_i} = 3 \cdot 0.5T_{sw} + T_{sw} = 4T_{sw} = 0.5ms$$

By doing this approximation the open loop transfer function for the i_{s_d} loop becomes:

$$G_{ol_d} = \frac{k_{p_d}}{\tau_d \cdot s} \cdot \frac{1}{R_s(T_{s_i}s + 1)} \tag{3.26}$$

Comparing the obtained open loop transfer function with the generic open loop transfer function for a second order system(based on the OM criterion), presented in Eq.3.16, the gain of the PI controller can be obtained.

$$\frac{k_{p_d}}{R_s \cdot \tau_d} = \frac{1}{2T_{s_i}} \Rightarrow k_{p_d} = R_s \frac{\tau_d}{2T_{s_i}} = 0.0289 \quad (3.27)$$

The resulting transfer function of the PI current controller, for the d current loop has the following expression:

$$PI_d = \frac{0.0289(1 + 0.003s)}{0.003s} = 0.0289 + \frac{9.6333}{s} \quad (3.28)$$

The Bode diagram for the i_{s_d} open loop is presented in Fig.3.19

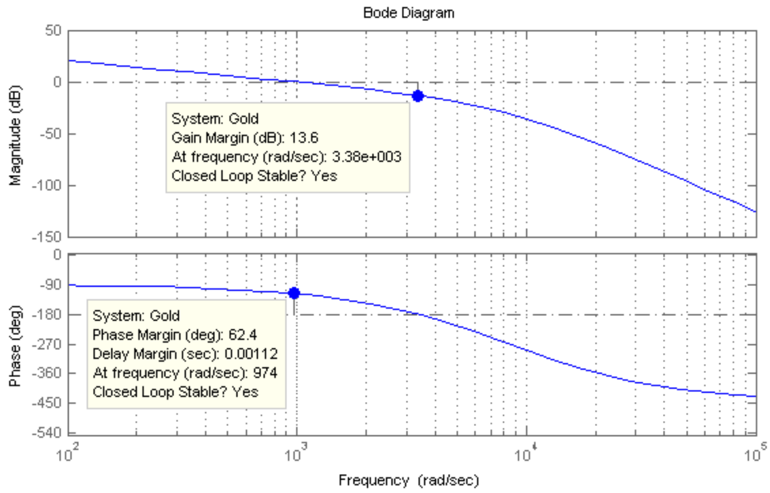

Figure 3.19: *Bode plot for the i_{s_d} loop*

As shown in Fig.3.19 the i_{s_d} closed loop is stable. The system is characterized by a gain margin of GM=13.6db, and a phase margin of PM=62.4deg. The step response of the closed loop system is plotted in Fig.3.20

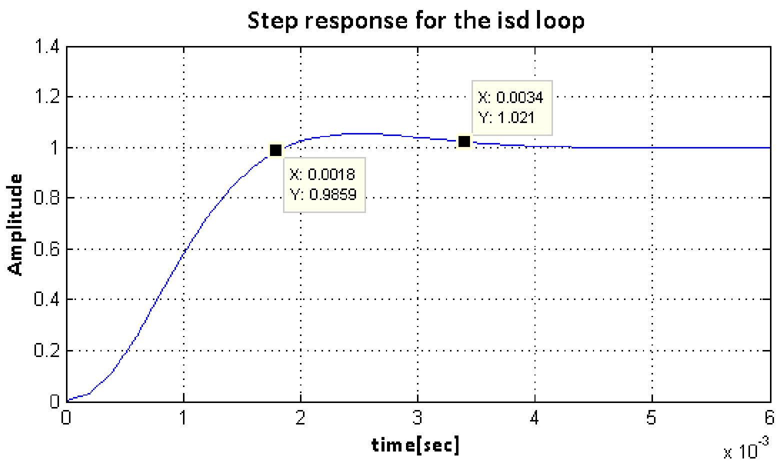

Figure 3.20: *Step response for the i_{s_d} loop*

The step response is characterized by the following parameters:

- rise time t=1.8ms
- settling time t=3.4ms
- maximum overshoot Mp=5.2%

Following the same algorithm like for de i_{s_q} loop, the d current closed loop can be estimated like a first order transfer function. The time constant of the transfer function is the same as for the d current loop, T_{id}=T_{iq}=0.9ms.

3.4.3 Tuning the speed controller

In order to tune the PI parameters of the speed controller, the plant of the IPMSM, needs to be known. The plant of the IPMSM from the speed point of wiew is calculated from the mechanical equation of the IPMSM, presented in Chapter2.

$$T_e - T_l - B \cdot \omega_m = J \cdot \frac{d\omega_m}{dt}$$

If the viscous friction coefficient is neglected, then the mechanical equation, in the 's' domain has the following shape:

$$T_e(s) - T_l(s) = \frac{J\omega_e(s)}{p_b} \cdot s \tag{3.29}$$

$\omega_e = p_b\omega_m$ is the electrical speed

Thus the transfer function of the IPMSM plant is:

$$\frac{\omega_e(s)}{T_e(s) - T_l(s)} = \frac{p_b}{Js} \tag{3.30}$$

The design of the speed loop is presented in Fig.3.21

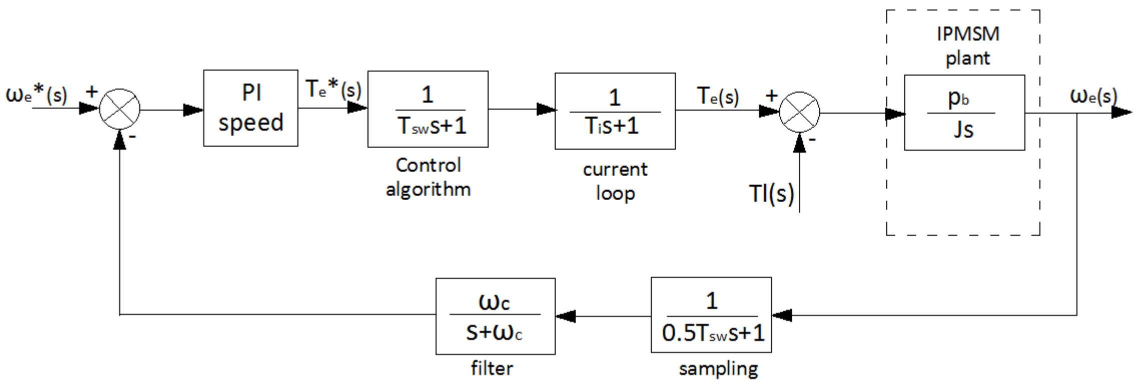

Figure 3.21: *Design of the speed loop*

The same as for the current loops, the speed controller was tuned in the continuos domain. Delays, expressed as a first order transfer function, have been introduced due to the delays from the real-life system. These delays are:

- the delay due to the digital calculation(control algorithm); the time constant of the first order transfer function is $T_{sw}=\frac{1}{f_{sw}}$=0.2ms(f_{sw}=5kHz is the switching and also sampling frequency used in the real-time application);
- the delay due to the current loops; as shown before, the first order approximation of the 2 current loop, has the same time constant $T_i=T_{id}=T_{iq}$=0.9ms;
- the delay due to the sampling; the delay is introduced by a first order transfer function that has the time constant equal to 0.5*T_{sw}=0.1ms ;
- the delay due to the filtering of the measured speed; an incremental encoder is used to measure the speed, so a digital filter is used to filter the speed; the filter has a cut-of frequency equal to ω_c =$2\pi f_c$=$2\pi 200$[Hz]=1256.6 $\frac{rad}{sec}$

The transfer function of the PI, for the speed loop is:

$$PI_\omega = k_{p_\omega} \frac{1+\tau_\omega \cdot s}{\tau_\omega \cdot s} \tag{3.31}$$

There are two inputs to the speed loop: the reference electrical speed ω_e and the load torque, T_l which is viewed as a disturbance. The control system is considered linear therefore the superposition principle ca be applied. First the speed is considered as an input while T_l=0. Second, the load T_l is considered as an input, while ω_e=0.[PED9]

The speed loop for the first case with unity feedback, when the speed is considered as input is presented in Fig.3.22.

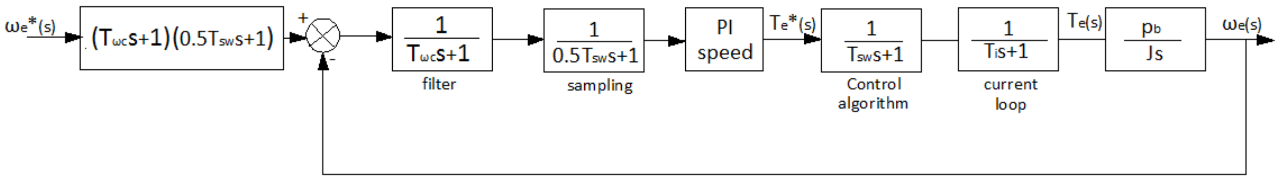

Figure 3.22: *Design of the speed loop when T_l=0*

where:

$T_{wc}=\frac{1}{\omega_c}$ is the time constant of the filter transfer function.

For this case only the proportional gain k_{p_ω} is considered.[PED9]. Thus the open loop transfer function has the following expression:

$$G_{ol_\omega} = k_{p_\omega} \cdot \frac{1}{0.5T_{sw}s+1} \cdot \frac{1}{T_{sw}s+1} \cdot \frac{1}{T_{wc}s+1} \cdot \frac{1}{T_is+1} \cdot \frac{p_b}{Js} \tag{3.32}$$

The root locus of the open loop transfer function is presented in Fig.3.23. As shown in the root locus plot, the system is unstable for a gain higher than k_{p_ω}=5.85. In order to find the gain of the PI speed controller, all the time constants of the delays are approximted to one time constant, simplifying the open loop transfer function.

$$T_{speed} = 1.5T_{sw} + T_i + T_{wc} = 2ms \tag{3.33}$$

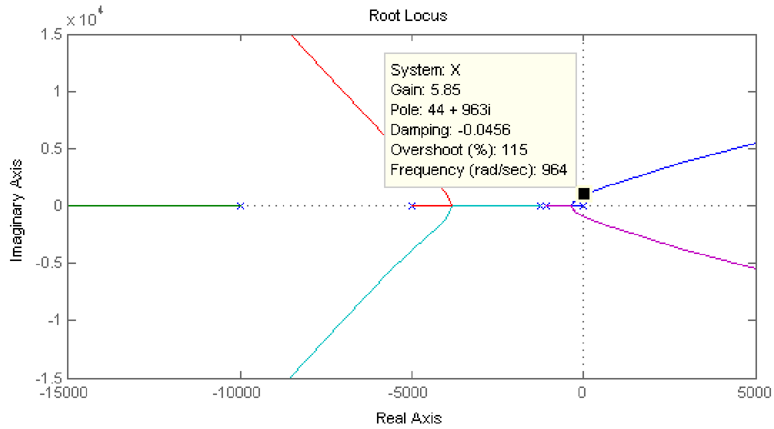

Figure 3.23: *Root locus for the speed open loop transfer function*

Taking this into account the speed open loop transfer function becomes:

$$G_{ol_\omega} = k_{p_\omega} \cdot \frac{1}{T_{speed}s + 1} \cdot \frac{p_b}{Js} \tag{3.34}$$

By comparing the obtained open loop transfer function with the generic open loop transfer function, for a second order system,(presented in Eq.3.16), based on the OM criterion, the gain of the PI speed controller can be found.

$$k_{p_\omega} \cdot \frac{p_b}{J} = \frac{1}{2T_{speed}} \Rightarrow k_{p_\omega} = \frac{J}{2p_bT_{speed}} = 0.8404 \tag{3.35}$$

In order to find the integral gain of the PI transfer function, the load torque of the machine T_l is considered an input while the speed is kept ω_e=0. Taking this into account, and introducing also the equivalent time constant T_{speed} for all the delays, the speed loop from Fig.3.21 has the following shape:

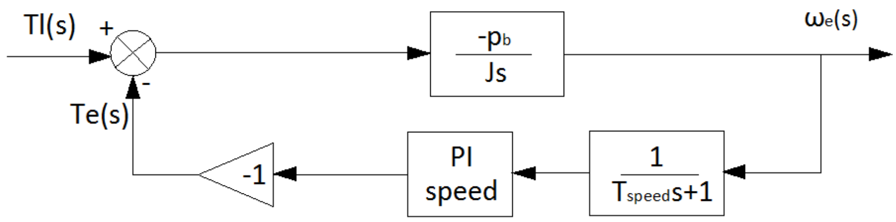

Figure 3.24: *Design of the speed loop when ω_e*=0*

The closed loop transfer function for the system presented in Fig.3.24 has the following expression:

$$\frac{T_l(s)}{\omega_e(s)} = \frac{\frac{-p_b}{Js}}{1 + \frac{-p_b}{Js} \cdot k_{p_\omega} \frac{1+\tau_\omega \cdot s}{\tau_\omega \cdot s} \frac{1}{T_{speed} \cdot s+1}} \tag{3.36}$$

Substituting the value of the gain of the PI controller, from Eq.3.35, into the closed loop transfer function from Eq.3.36, and simplifying the expression, the following equation is obtained:

$$\frac{T_l(s)}{\omega_e(s)} = \frac{\frac{-p_b\tau_\omega}{J} \cdot T_{speed} \cdot s(T_{speed} \cdot s + 1)}{2T_{speed}^2\tau_\omega \cdot s^3 + 2T_{speed}\tau_\omega \cdot s^2 + \tau_\omega \cdot s + 1} \tag{3.37}$$

Using the Symmetric Optimum(SO) method for tuning the PI controller[Mizera,2005], τ_ω can be obtained:

$$\tau_\omega^2 - 4\tau_\omega \cdot T_{speed} = 0 \Rightarrow \tau_\omega = 4T_{speed} = 0.008 \tag{3.38}$$

The transfer function of the PI speed controller is found:

$$PI_\omega = 0.8404\frac{1 + 0.008 \cdot s}{0.008 \cdot s} = 0.8404 + \frac{105.05}{s} \tag{3.39}$$

The step response of the speed loop is presented in Fig.3.25. After 0.15sec, a step in the load was applied to see how the disturbance affects the speed loop.

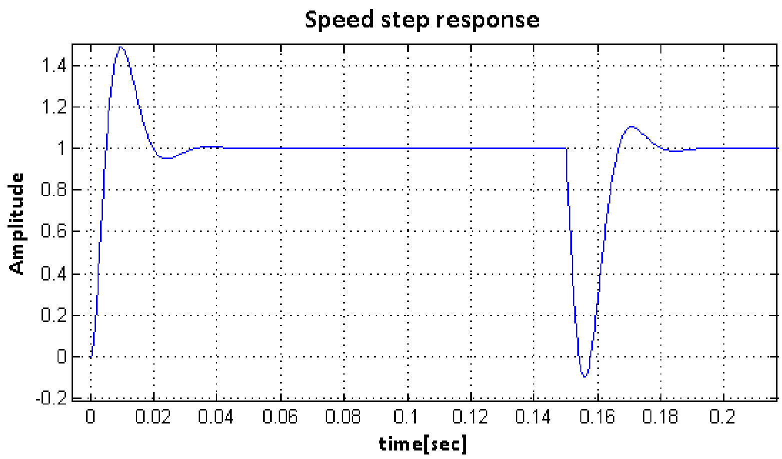

Figure 3.25: *Step response for the speed loop*

The characteristics of the speed loop step response are:

- rise time t=5ms
- settling time t=40ms
- maximum overshoot Mp=48.5%
- after the load step is applied, the speed settling time is t=40 ms.

The overshoot of the speed controller is almost 50%. When the speed controller is implemented in the field oriented control, this overshoot will be translated into a very big torque command which will cause high currents, above the maximum current. Therefore the PI speed controller is designed with anti-windup, and the currents are limited to the maximum available ones. The anti wind-up on the speed controller will also determine a slower response of the speed controller.

3.4.4 Discrete PI controller design

The PI controllers, for the two current loops, and for the speed loop were implemented in discrete time as well. Using the zero-hold method for discretization, with the sampling frequency of T_{sw}=5kHz, the following PI discrete transfer functions were obtained:

- for the q current loop PIq_d=0.0471$\cdot$ $\frac{9.6 \cdot T_{sw}}{z-1}$
- for the d current loop PId_d=0.0289$\cdot$ $\frac{9.65 \cdot T_{sw}}{z-1}$
- for the speed loop $PI\omega_d$=0.8404$\cdot$ $\frac{105 \cdot T_{sw}}{z-1}$

In order to check the step response for the q current loop, the loop from Fig.3.10 was transformed into discrete time. The discrete i_{s_q} loop is presented in Fig.3.26 The step

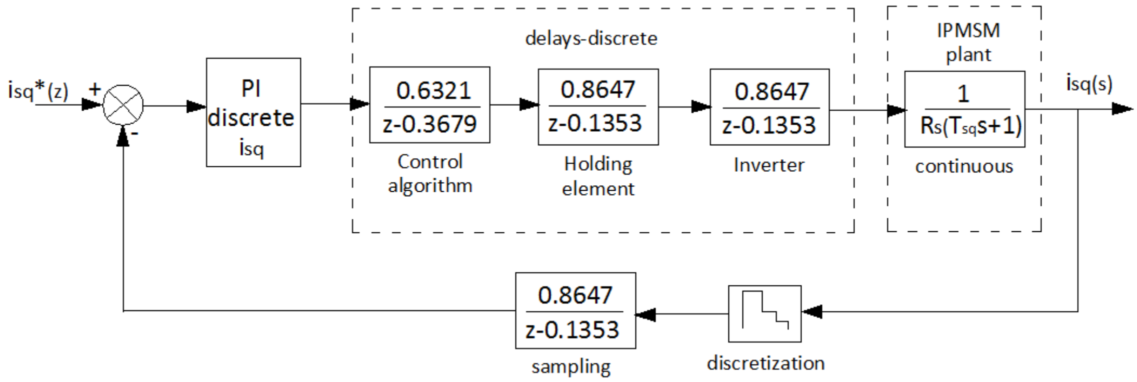

Figure 3.26: *Design of the i_{s_q} discrete current loop*

response from the simulation model and also from the experimental setup are presented in Fig.3.27. For the experimental test, a step of i_{s_q}=5A, was given.

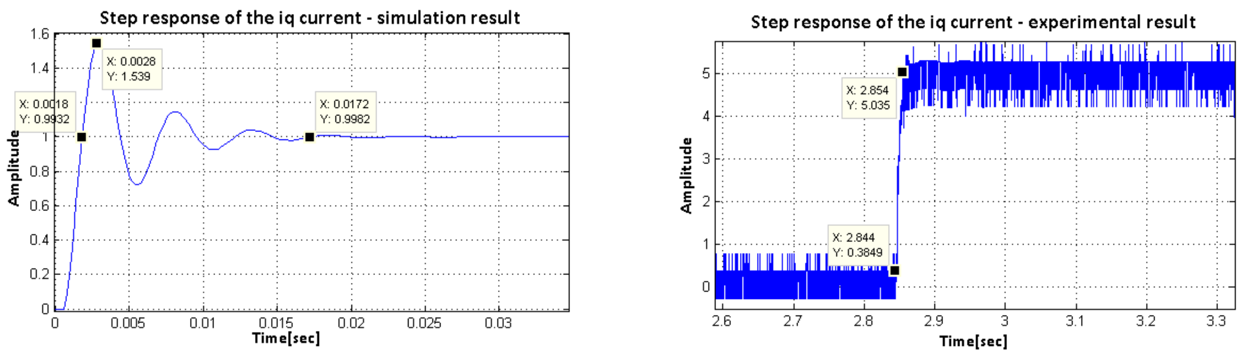

Figure 3.27: *Step response of the i_{s_q} loop- simulated and experimental*

The rise time of the simulated discrete step response for the q current, is the same as for the continuous simulation, t=1.8ms. Still the maximum overshoot is bigger, Mp= 53.9%. The settling time is also higher than for the continuous simulation, t=17ms. From the experimental test, the settling time of the q current is t=11ms, which is smaller than the simulated value. The cause of the difference between the simulated and the experimental results may be the choosing of the delays that were introduced in the design of the q current loop. The delays chosen during the design of the controller are not the same as the delays in the real system. The noise on the experimental curve is due to the noise in the measurement of the current.

The i_{s_d} current loop was also discretized. The discretized d current loop is presented in Fig.3.28 The simulated step response of the i_{s_d} discrete loop, and also the experimental

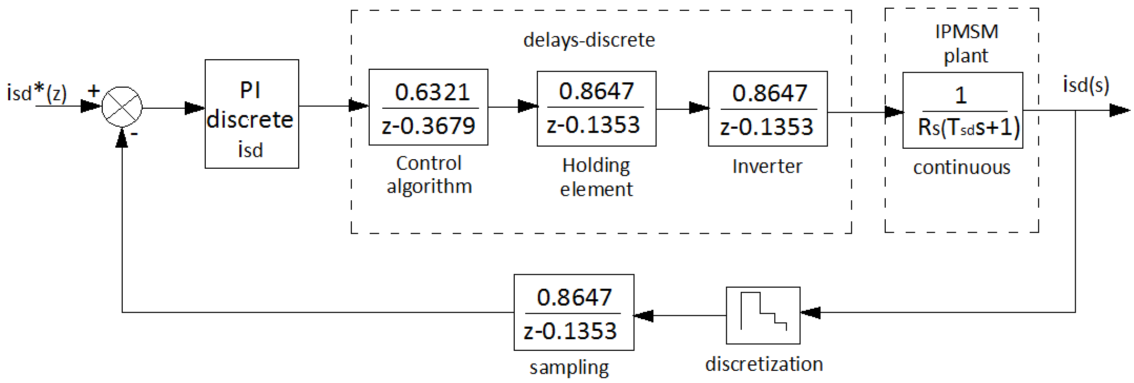

Figure 3.28: *Design of the i_{s_d} discrete current loop*

result, is plotted in Fig.3.29. For the experimental test, a step of i_{sd}=-5A was given.

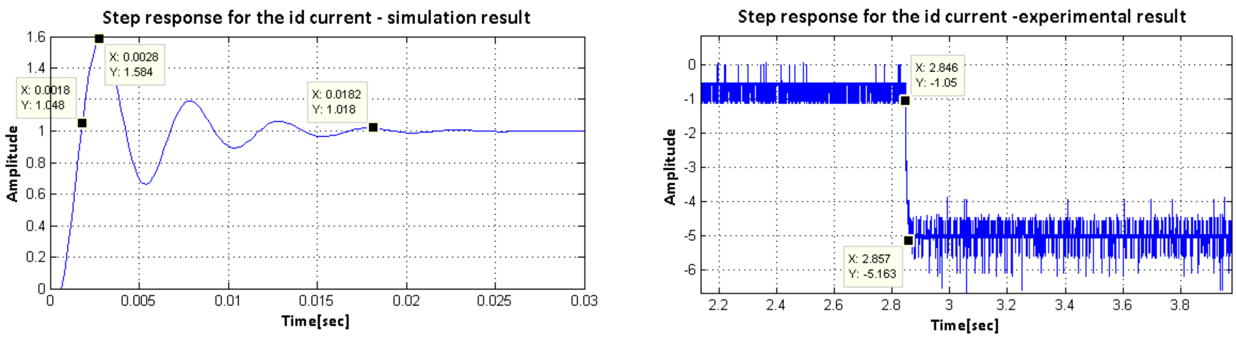

Figure 3.29: *Step response of the i_{s_d} loop- simulated and experimental*

The rise time of the simulated discrete step response is the same as for the continuous simulation, t=1.8ms. The maximum overshoot, is higher than for the continuous simulation, Mp=58.4%. So is the settling time, t=18ms. Taking a look at the experimental result, the rise time is smaller than the simulated one, and is the same as for the q current loop, t=11ms. The difference between the simulated and experimental results may be the same, the delays that were introduced for the design of the d current loop. The noise on the experimental step response is due to the noise in the measurement of the current.

The step response of the speed loop was also checked in a discrete-time simulation. The structure of the discrete speed loop is presented in Fig.3.30. The simulated step response is presented in Fig.3.31

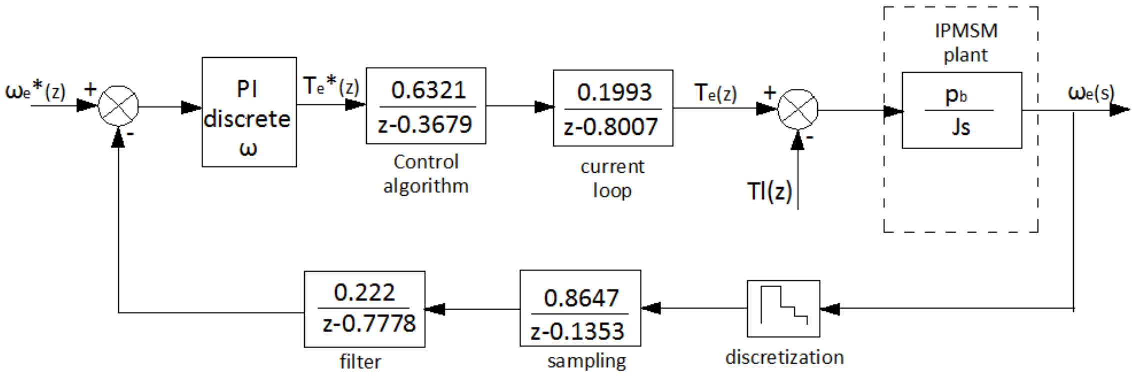

Figure 3.30: *Design of the discrete speed loop*

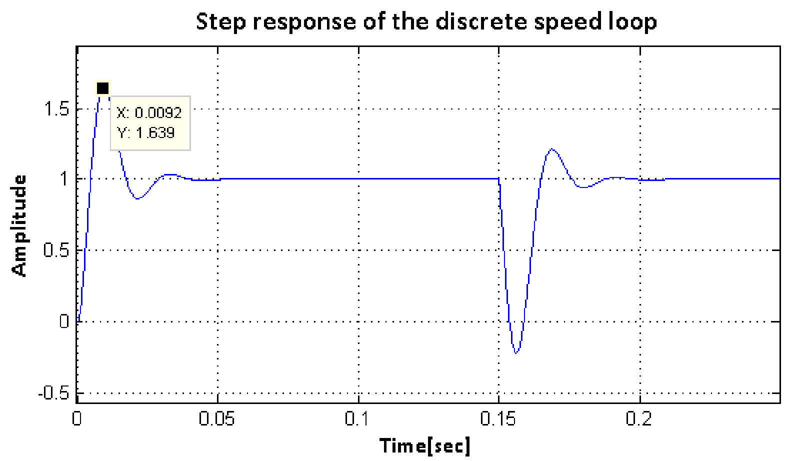

Figure 3.31: *Step response of the discrete speed*

The discrete step response is characterized by the following parameters:

- rise time t=5ms
- settling time t=50ms
- maximum overshoot Mp=63.9%
- after a step load is applied after 0.15sec, the settling time is t=50ms

The rise time is the same as for the continuous simulation, but the maximum overshoot and settling times are bigger than the continuous simulation.

3.4.5 Anti-windup structure for the PI controllers

The dq reference voltages, given by the output of the PI current controllers are limited. The value of the DC link of the inverter used is 24V. Therefore the voltage is limited to the maximum available voltage from this DC link value, before going into overmodulation. The dq currents are also limited to the maximum alowable value, given by the maximum value of the inverter. The limitation of the currents is translated into a limitation of the produced torque.

Due to these limitations of the voltages and currents in the control, the PI controllers need to have anti-windup. When the controlled values(currents and voltages) are saturated, the anti-windup prevents delays in the responses of the PI controllers. The structure of the PI with anti wind-up, for the current loops is presented in Fig.3.32[Franklin,2006]

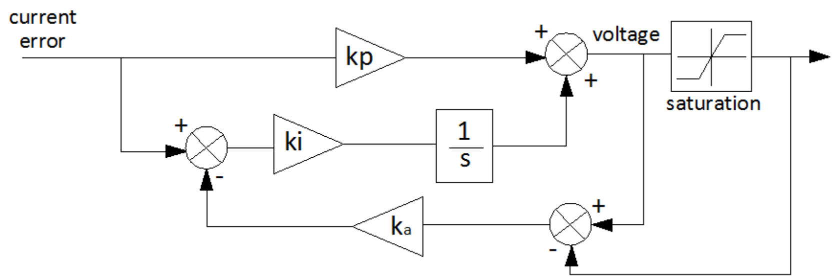

Figure 3.32: *PI current regulator with anti-windup*

where:

k_a is the anti-windup gain for the current loops

The impact of the anti-windup is on the integrator of the PI controller. When the output of the PI is saturated, the integration effect of the PI is lowered. The structure of the PI with anti-windup, for the speed controller is presented in Fig.3.33

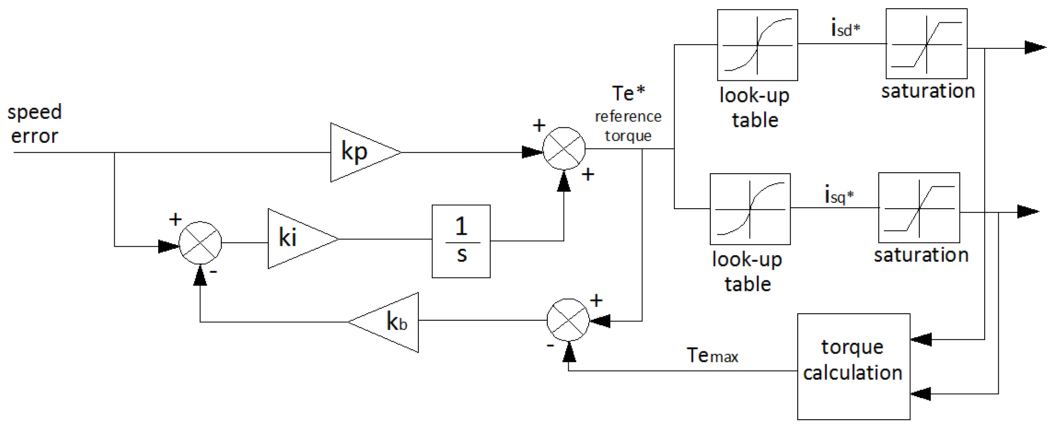

Figure 3.33: *PI speed regulator with anti-windup*

where:

k_b is the anti-windup gain for the speed loop

The output of the PI speed controller is a reference torque command. Using the implemented look-up table, for MTPA control, the reference ${i_{s_d}}^*$ and ${i_{s_q}}^*$ currents are found. These currents are limited. From the limitation of the currents, a maximum torque can be calculated and used for the speed anti-windup. The anti-windup gains k_a and k_b chosen are:

- k_a=1
- k_b=2

3.5 Field Weakening Algorithm

The speed of the IPMSM motor is controlled through an indirect FOC. When performing this control, the currents and voltages are kept below a maximum value. The maximum current and voltage are usually set by the maximum current of the inverter, and maximum available voltage from the DC link. These two constraints, maximum available current and maximum available voltage, can be expressed like the following[Sul,2003]:

$$i_{s_d}^2 + i_{s_q}^2 \leq I_{max}^2 \tag{3.40}$$

$$u_{s_d}^2 + u_{s_q}^2 \leq U_{max}^2 \tag{3.41}$$

where:

- I_{max} is the maximum inverter phase-current amplitude
- U_{max} is the maximum phase-voltage amplitude from the inverter

Using the dq dynamic voltage equations of the IPMSM, and the dq flux equations, presented in 2, the steady state dq voltage equations can be written like in the following:

$$\begin{aligned} U_{s_d} &= Rs \cdot i_{s_d} - \omega_e \cdot L_q \cdot i_q \\ U_{s_q} &= Rs \cdot i_{s_q} + \omega_e \cdot (L_d \cdot i_d + \Psi_m) \end{aligned} \tag{3.42}$$

If the stator resistance is neglected, by substituting the d and q voltage equations in the voltage constraint from Eq.3.41, the following expression is obtained[Sul,2003]:

$$(\frac{U_{max}}{\omega_e})^2 \geq L_d^2 \cdot (\frac{\Psi_m}{L_d} + i_{s_d})^2 + (L_q \cdot i_{s_q})^2 \tag{3.43}$$

Eq.3.43 represents an ellipse, whose centre is situated at I_{inf}=($\frac{-\Psi_m}{L_d}$,0). This point is called infinite speed point, and it represents the value of the stator current at which the speed of the motor is theoretical infinite[Soong,1994]. When the speed of the motor ω_e is increasing, the radius of the ellipse is decreasing, shrinking towards the center point. This ellipse equation (that represents the voltage limit), together with Eq.3.40, which is a circle with constant radius(that represents the current limit) can be mapped into the (i_{s_d},i_{s_q}) plane, for an IPMSM. The (dq) representation of the two constraints is presented in Fig.3.34

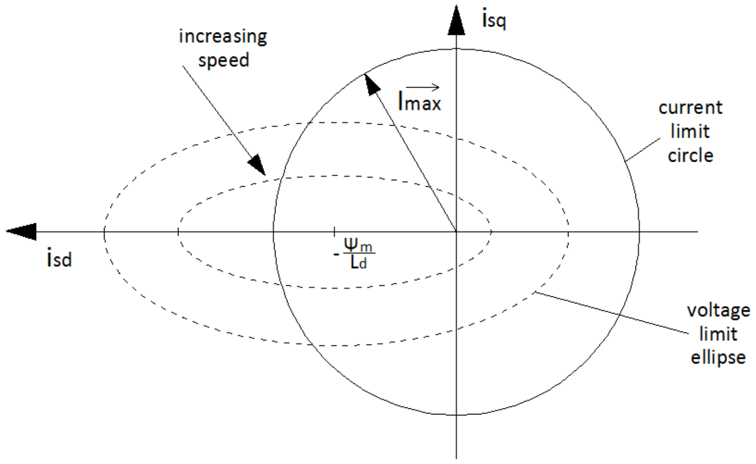

Figure 3.34: *i_{dq} representation of the voltage and current limitation*

The amplitude of the stator current is limited to I_{max}=300A. Using the parameters for the Sauer-Danfoss IPMSM, the centre of the voltage limitation ellipse can be calculated.

$$I_{inf} = \frac{-\Psi_m}{L_d} = 338.32A \tag{3.44}$$

The centre of the voltage limit ellipse is situated outside the limit circle(I_{max}=300A). Theoretically it means that the 'infinite' speed of this particular motor cannot be reached. The i_{sd} representation of the voltage and current limitations, can be used as a tool to investigate the maximum speed, and torque of the IPMSM.

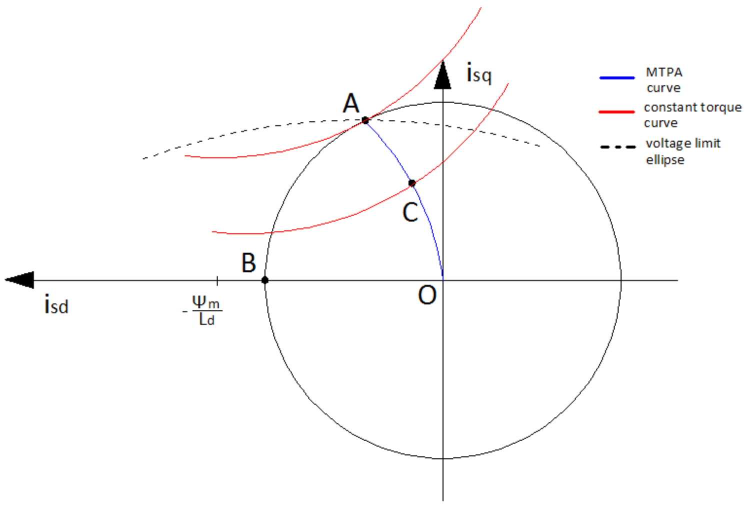

Figure 3.35: *i_{dq} representation of the voltage and current limitation for the Sauer-Danfoss IPMSM* [Morimoto,1990]

As shown in Fig.3.35, starting from 0 speed on the MTPA curve, the speed of the motor can be increased until the base speed, ω_b, which is represented by point A, that is given by the intersection of the current limit circle and voltage limit ellipse. Within the area ABO (delimited by the current limit circle, voltage ellipse and the MTPA) the current vector can take any value, without violating the voltage or the current limit.

When the speed of the motor reaches the base speed, the voltage and current limit are reached. From the torque production point of view, the maximum torque $T_{e_{max}}$ is also given by the currents in the working point A(i_{s_d},i_{s_q}). On the OA curve the motor can be operated at constant torque, equal to the maximum value[Soong,1994]

Using the simple field oriented control the speed of the motor cannot be increased above the base speed. The speed of the motor can be further increased, if a Field Weakening(FW) control is implemented. The area delimited by the ABO points, is the locus of the stator current in field weakening. The idea of a field weakening algorithm is to lower the resulting d flux by reducing the effect of the flux of the permanent magnets. This is done by increasing the real component of the stator current i_{s_d}. Looking at d flux equation,

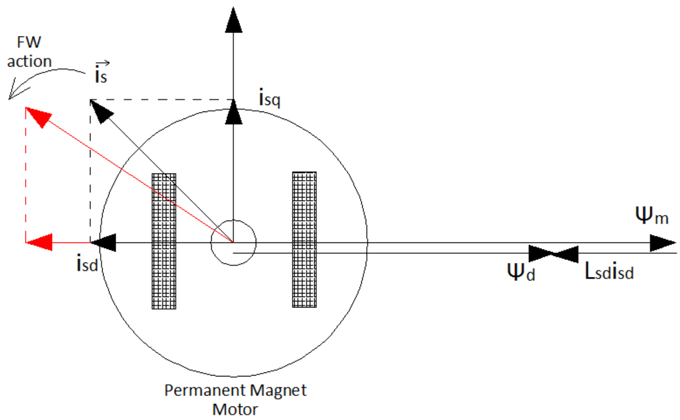

Figure 3.36: *Vector diagram illustrating the resulting flux linkage[Soong,1994]*

$$\Psi_d = L_d \cdot i_d + \Psi_m$$

if the i_{s_d} current is increased (towards the negative side for the motoring quadrant of the IPMSM), the resulting Ψ_d flux is decreased. By lowering the resulting flux the speed of the machine can be increased above the base speed.

If the filed weakening is triggered before the voltage and current limits are active, like point C in Fig.3.35, then field weakening can be achieved by moving the current vector along the constant torque line. If field weakening is triggered when the voltage and current limits are reached, point A, then field weakening can be achieved by moving the current vector along AB curve. As the speed of the motor is increased, the ellipse radius decreases, and the working point is given by the intersection of the current limit circle and the voltage limit ellipse. On AB curve, field weakening can be achieved with constant maximum power.[Soong,1994]

The field weakening control implemented was proposed by J.Way and T.Jahns in [Jahns,2001]. The structure of the control is presented in Fig.3.37.

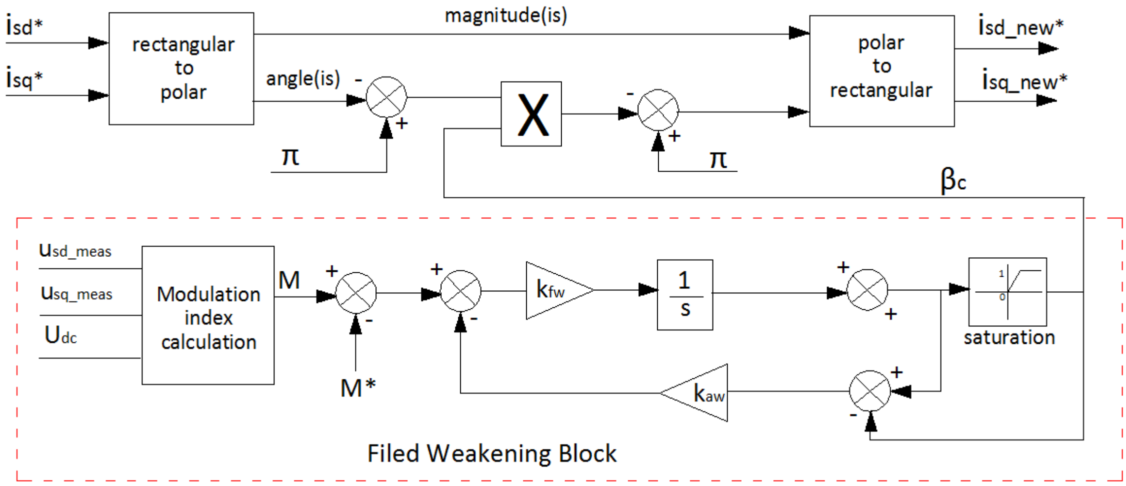

Figure 3.37: *FW control structure*

where:

M is the calculated modulation index

M* is the threshold value of the modulation index

β_c is a coefficient between (0..1)

U_{dc} is the DC-link voltage of the inverter

k_{fw} is the gain of the FW integrator

k_{aw} is the anti-windup gain

The FW controller, like presented in Fig.3.37 is a pure integrator with anti-windup. In order to perform this FW control, the *dq* voltages have to be measured, and also the DC-link voltage of the inverter. Based on this measured values the modulation index can be calculated. The modulation used is 2-level Space Vector Modulation, for which the modulation index can be calculated according to:

$$M = \frac{\sqrt{3}\sqrt{u^2_{sd_{meas}} + u^2_{sq_{meas}}}}{U_{dc}} [\text{Wu2006}] \tag{3.45}$$

The error between the measured and the threshold value of the modulation index M*, is fed to an integrator with anti-windup. The output of the integrator β_c, which is limited between (0..1) is multiplied with the complementary angle of the stator current vector. When the difference between the measured and the threshold value of the modulation index is bigger than 0, then β_c=1, and the angle of the current remains unchanged. If the error is negative, the output of the integrator will immediately decrease below 1. This will result in a decrease of the angle of the stator current, and the motor will go into field weakening. The graphical representation of the FW action, is presented in Fig.3.38

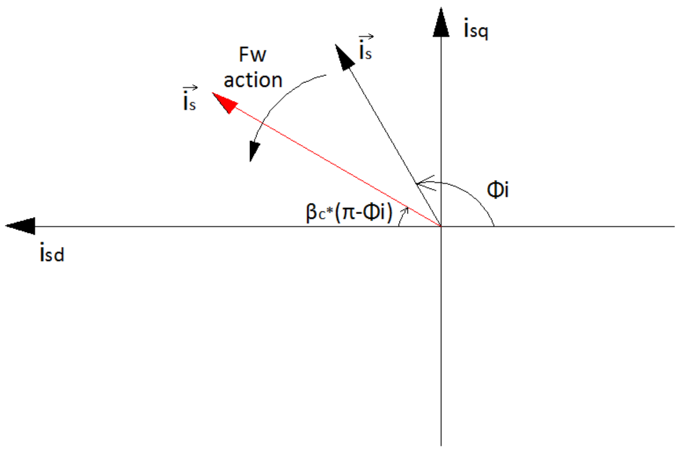

Figure 3.38: *FW action of the implemented control*

where:

ϕ_i is the angle of the current vector

The onset of the FW control is dictated by the reference modulation index M*. When going into field weakening mode, there is a high risk of saturating the current regulators(PI's for i_{s_d} and i_{s_q}). If the current controllers are saturated, the control over the motor is lost, due to the fact that there is no more voltage available to run the motor at the required currents.

The modulation index M can be used as an indicator of the current regulator saturation, when it approaches M=1. So by setting the threshold value of the modulation index close to 1, in the FW algorithm, the saturation of the current controllers can be overcomed.[Jahns,2001]

When operating in FW mode, if the measured modulation index decreases(due to decrease in load or speed) bellow the threshold value, then the output of the integrator quickly rises to 1, and the motor goes out of FW.

The chosen values for the integrator and anti-windup gain are:

- k_{fw}=1500
- k_{aw}=1

3.6 Simulation results

The Field Oriented Control designed, together with the Field Weakening Control, were tested in Matlab/Simulink as a discrete simulation model. The electrical parameters of the IPMSM used for the simulation model are the same as presented in Table2.1, in Chapter2. For simplicity, from the mechanical parameters calculated, only the moment of inertia J was used. Space vector modulation was used as a control technique for the inverter. A SVM model block, from the dSpace Laboratory, at IET, was used. The sampling time of the simulation model was T_{sw}=0.0002ms(5KHz). The initialization file for the Simulink model is presented in Appendix A. The configuration of the simulation blocks is presented in Appendix C. The diagram overall simulation structure is presented in Fig.3.39

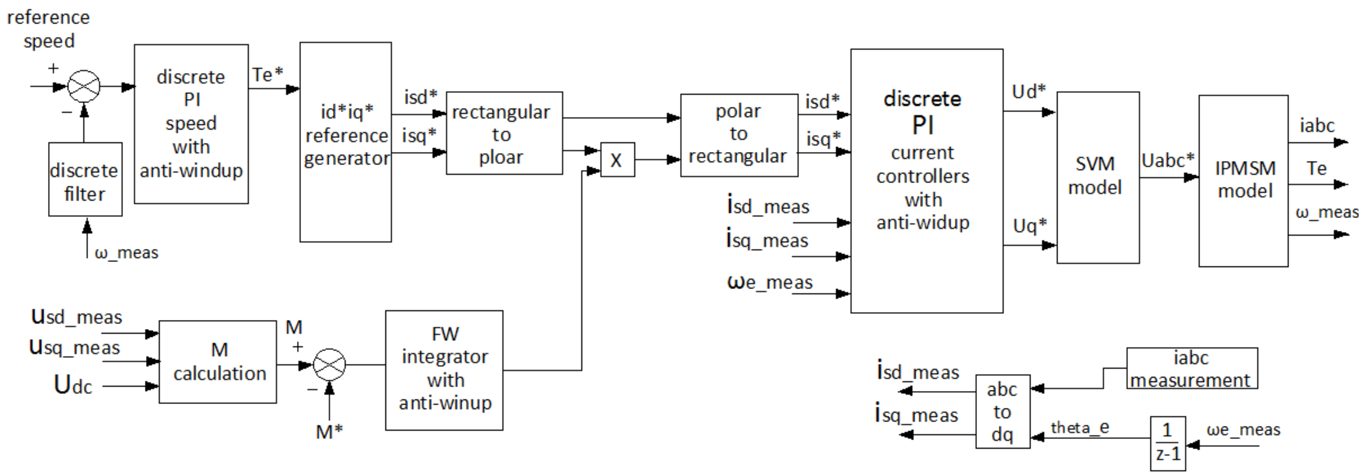

Figure 3.39: *FW action of the implemented control*

The following tests were performed on the designed simulation model:

- FOC test with no load
- FOC test at 10Nm load
- FOC test at 15Nm load
- FOC with Field Weakening

3.6.1 FOC test at no load

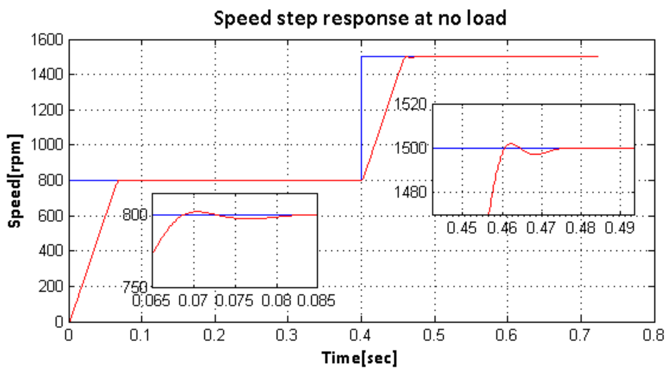

Figure 3.40: *Speed response at no load*

The first test of the FOC control was done at no load. At the starting point a step of 800rpm was given to the reference speed. After 0.4sec, another step of 700rpm was given to the reference speed. The plot showing the reference speed, and the response of the speed of the machine , is presented in Fig.3.40. As it can be depicted from the plot, the speed reaches 800rpm, in t=70 ms. The step from 800rpm to 1500 is reached in t=60ms. Due to the speed anti-windup the step response is lowered, but it results in a very small overshoot. The overshoot for the two steps, is less than 5rpm(≈0.6%).

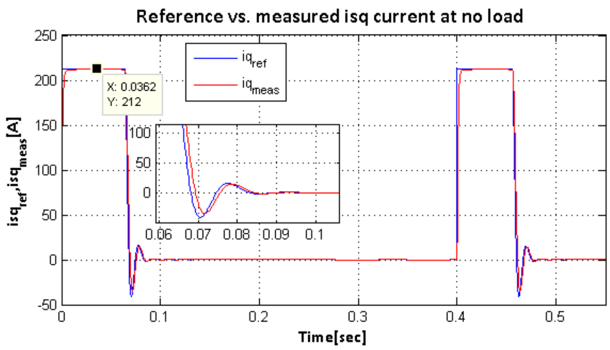

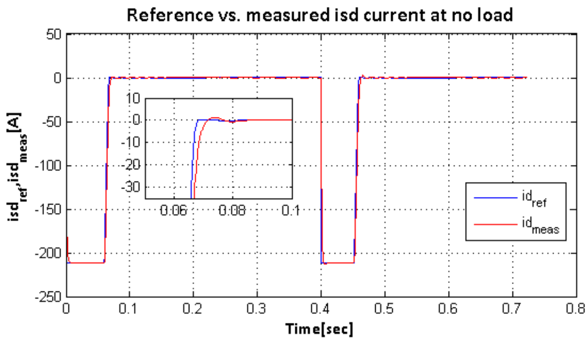

Figure 3.41: *Reference* dq *currents vs. measured* dq *currents*

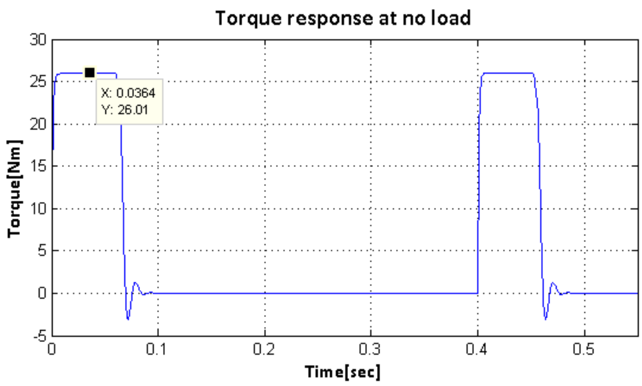

Figure 3.42: *Torque response at no load*

The dq reference and measured currents are plotted in Fig.3.41. As it can be depicted from the plot, both currents d and q, follow with very good accuracy the reference currents. At the starting point, i_{s_d} and i_{s_q} are limited both at$|i|$=212A. The limitation is done in the FOC control. This limitation is translated into a torque limitation as it can be seen in Fig.3.42. The starting(acceleration torque) is limited to Te=26.01Nm. Once the motor reaches the reference speed(800rpm), the currents stabilize at 0A, which of course corresponds to Te=0. It is the same situation when the second step, to 1500rpm is made. The currents, and the torque are limited at the same values, until the motor reaches the reference speed.

The locus of the current vector $\vec{i_s}$ is shown in Fig.3.43. From the figure it can be seen the route of the current vector from the starting point at (0,0), to the maximum torque point (i_{s_d},i_{s_q})=(-212, 212)A. During the acceleration periods the current does not follow the MTPA curve, due to the fact that for both d and q currents, the same limit value was set. After the current limitations become inactive, the current vector follows the MTPA curve down to Te=0.

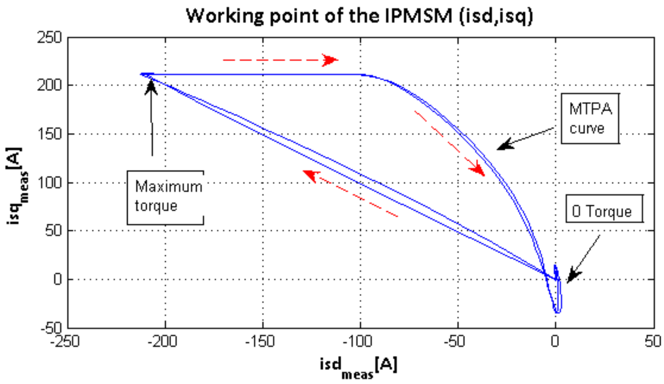

Figure 3.43: *Representation of the stator current vector*

The *dq* voltages are shown in Fig.3.44. The u_{s_d} voltage is zero in both steady-state cases, at 800rpm, and 1500rpm. Therefore the u_{s_q} voltage is equal to the amplitude of the stator phase voltage. At 800rpm u_{s_q}=4.8V, and at 1500r pm u_{s_q}=9.15V.

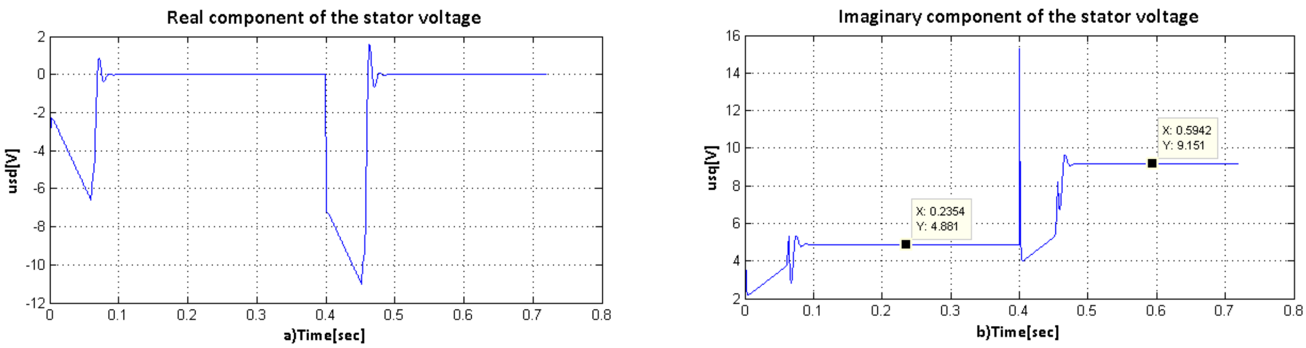

Figure 3.44: *Plot of a)u_{s_d} voltage and b)u_{s_q} voltage*

3.6.2 FOC test at 10 Nm load

For the second test the same procedure was followed: at the beginning a step in reference speed of 800rpm, followed by another step until 1500rpm. This time the motor was loaded to 10Nm. The speed response of the motor is plotted in Fig.3.45. As expected, when the motor is loaded the rise time of the speed is slower than at no load. The rise time of the motor speed, at the step of 800rpm is t=110ms. The same for the second step of 700rpm, the rise time is t≈=90ms. Still the overshoot of the speed in both cases is smaller than Mp=5rpm≈=0.6%.

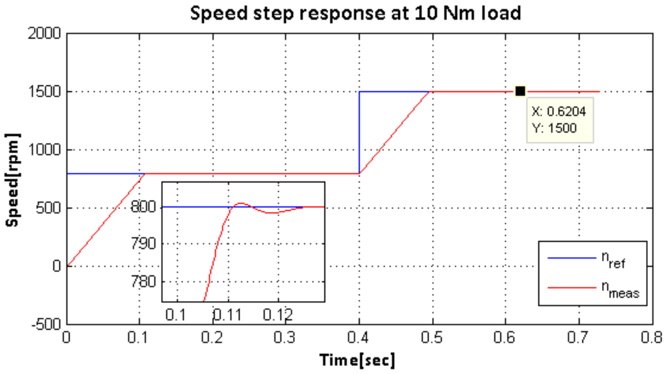

Figure 3.45: *Speed response at 10Nm*

The reference *dq* currents and the measured *dq* currents are plotted in Fig3.46. The same as the test at no load the measured currents follow the reference currents with very good accuracy. The maximum currents are also the same, given by the limitation imposed at 212A.

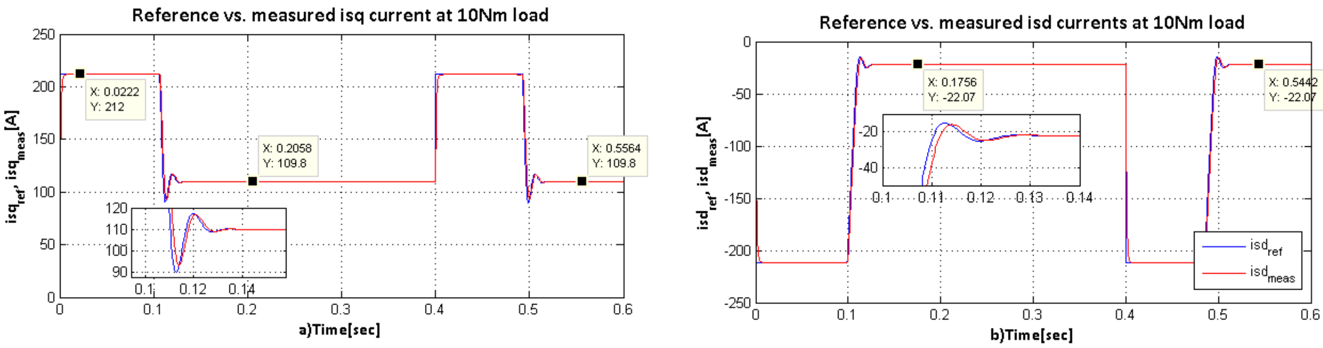

Figure 3.46: *Reference* dq *currents vs. measured* dq *currents*

The acceleration torque is limited to Te=26Nm, as it is presented in Fig.3.47, and is the same for both steps in speed. In the two steady state cases, at 800rpm and 10 Nm, and at 1500rpm and 10 Nm, the current working point is the same (i_{s_d},i_{s_q})=(-22.7, 109.8)A. This gives a phase current amplitude, at 10Nm, of Is=111A.

The dynamic behaviour of the stator current vector can be seen in Fig.3.48. At the beginning the motor starts with the maximum acceleration torque. Once the speed of the motor reaches 800rpm, the current vector follows the MTPA curve, and reaches a steady-state point at 10Nm. Then, after the reference speed is increased to 1500rpm, the motor is again accelerated with the maximum torque until the motor reaches the imposed speed. After 1500rpm are reached, the current vector follows the MTPA curve to the same steady-state point.

The *dq* voltages are presented in Fig.3.49. For the first steady-state point, at 800rpm, the d and q voltages are (u_{s_d},u_{s_q})=(-2.8, 5.6)V. This gives a magnitude for the stator phase voltage of U=6.2V. For the second-steady state point, the voltages are (u_{s_d},u_{s_q})=(-5, 9.6)V, that give an increased amplitude of U=10.8V.

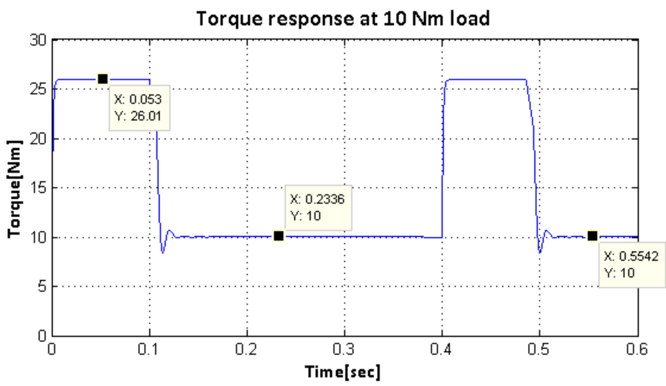

Figure 3.47: *Torque response at 10Nm load*

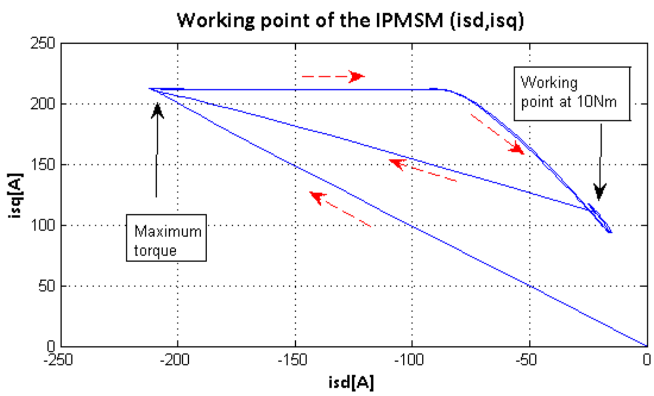

Figure 3.48: *Representation of the stator current vector*

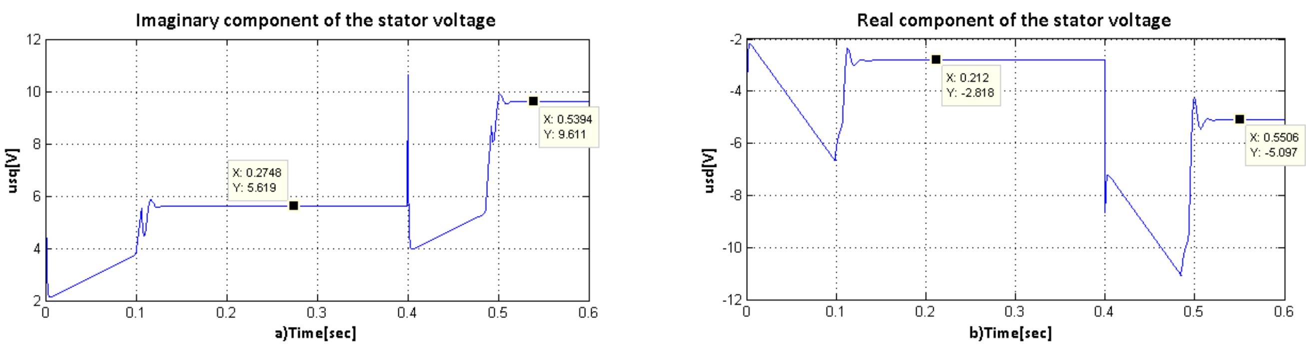

Figure 3.49: *Plot of a)u_{s_d} voltage and b)u_{s_q} voltage*

3.6.3 FW test with ramp reference speed at 10Nm load

For this test the threshold value for the modulation index is set to M*=0.99. The shape of the reference speed is presented in Fig.3.50. From the starting point, the speed of the motor is accelerated with a slope of 1000rpm/s, until it reaches a steady-state speed of 1500rpm. Using the same slope the speed is further increased until 2300rpm, followed by a decrease to 1800rpm. As shown in the plot the speed of the motor follows with very good accuracy the imposed speed.

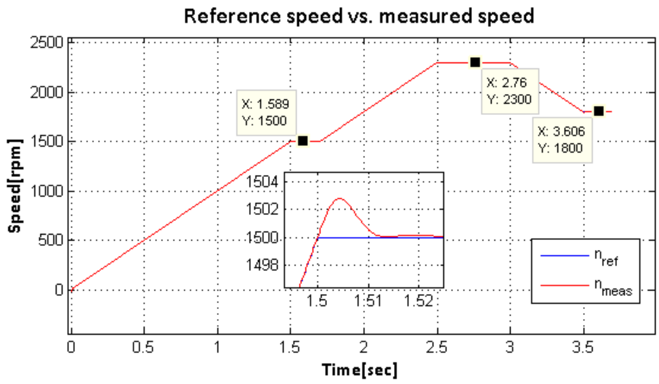

Figure 3.50: *Speed ramp response at 10Nm with FW*

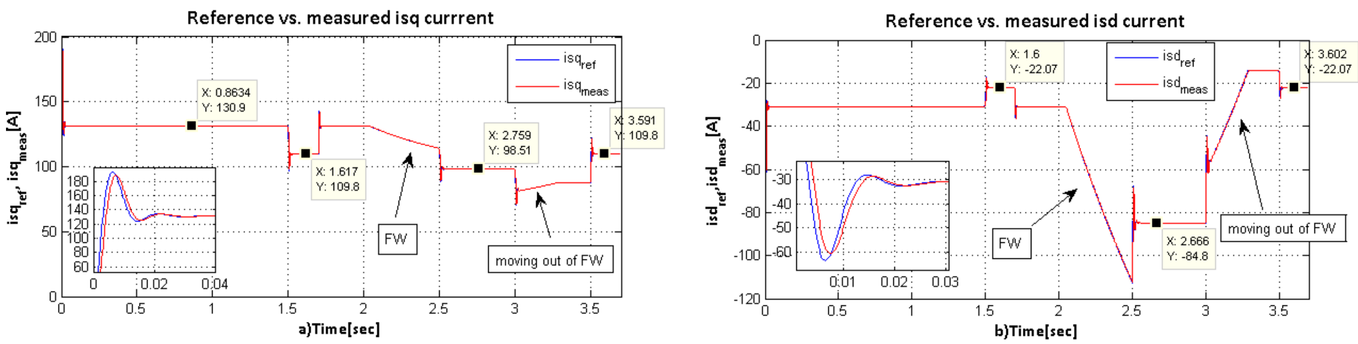

Figure 3.51: *Reference* dq *currents vs. measured* dq *currents*

Taking a look at the *dq* currents in Fig.3.51, the starting currents are not limited, due to the lower requirement of torque during the ramp acceleration. The acceleration torque is Te=12.11Nm, like presented in Fig.3.52, and it is given by the currents (i_{s_d},i_{s_q})=(-30.8, 130.9)A. After the motor reaches 1500rpm, the torque stabilizes at Te=10Nm, as expected. The currents in this working point are of course the same as for the previous case from Section3.6.2, when the motor was running at the same speed and torque. After 1.7sec, the speed of the motor starts to increase. As shown in Fig.3.52 the acceleration torque is the same as before and is constant until the speed reaches 2300rpm. At time t=2.04 the motor starts going into field weakening, as the i_{s_d} current starts to decrease.

The action of the FW algorithm is only on the angle of the stator current vector and not on the magnitude. As shown in Fig.3.51 when the motor goes into FW, and the i_{s_d} current is decreasing(negative side), the i_{s_q} current is also decreasing. This is due to the action of the speed controller that keeps the torque constant. The FW mode is triggered by the measured modulation index that reaches the set threshold value of M*=0.99, as shown in Fig.3.53a).

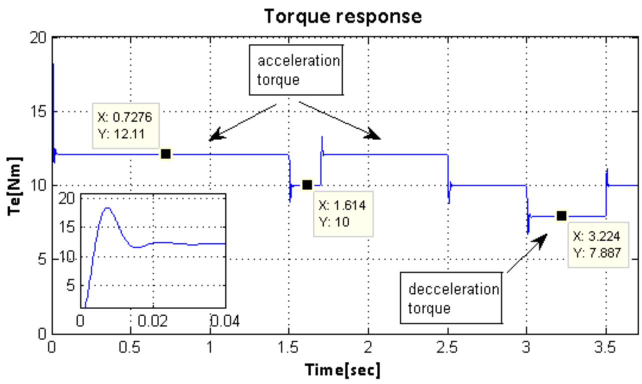

Figure 3.52: *Torque response at 10Nm load with FW*

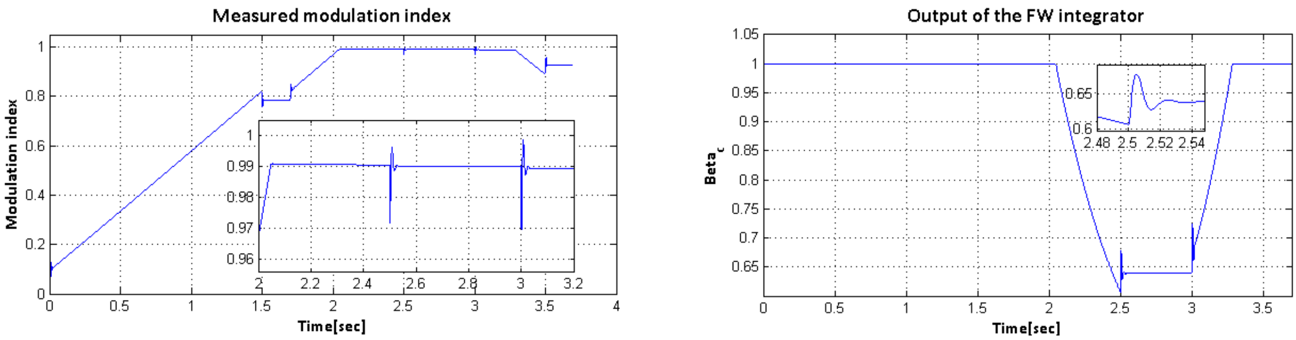

Figure 3.53: *Plot of a)the measured modulation index and b) the output β_c of the FW integrator*

As soon as the measured modulation index starts to increase above M*=0.99, the FW. integrator output starts to decrease below 1, and the motor goes into field weakening(Fig.3.53a)). When the speed reaches 2300rpm, the motor reaches a steady-state point in FW. The currents in this point are (i_{s_d},i_{s_q})=(-84.8, 98.51)A.

At time t=3 sec, the speed starts to decrease. As soon as the measured modulation index goes below the threshold value(at t=3 in Fig.3.53b), the motor starts to go out of field weakening, and the i_{s_d} current starts to increase. Also i_{s_q} increases, due to the fact that the motor goes out of FW at constant torque, as it can be seen in Fig.3.52 . After the speed reaches 1800rpm, the motor reaches the same steady-state point, out of FW, at 10Nm.

A graphical representation of the stator current vector is presented in Fig.3.54. The motor accelerates on the MTPA curve and it reaches the steady-state point, at 10 Nm. From this point, it can be clearly seen that the motor goes into FW on a constant torque curve(the constant acceleration curve), and it reaches a steady-state point in FW. It can also be seen that the motor goes out of FW on a constant torque curve(constant deceleration torque).

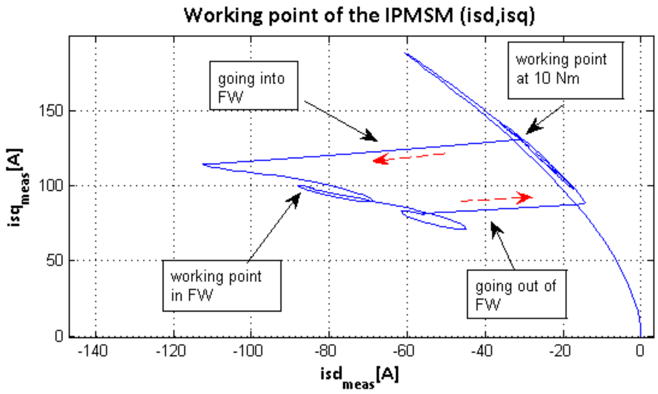

Figure 3.54: *Representation of the stator current vector*

3.6.4 FW test with step reference speed at 10Nm load

A second test was done to check the behaviour of the FW controller. The reference speed was set this time as steps, at a load torque of 10Nm. A first step is done to 1500rpm, followed by a step to 2200rpm, like presented in Fig.3.55. The behaviour of the control for the first step is the same as presented in Section3.6.2.

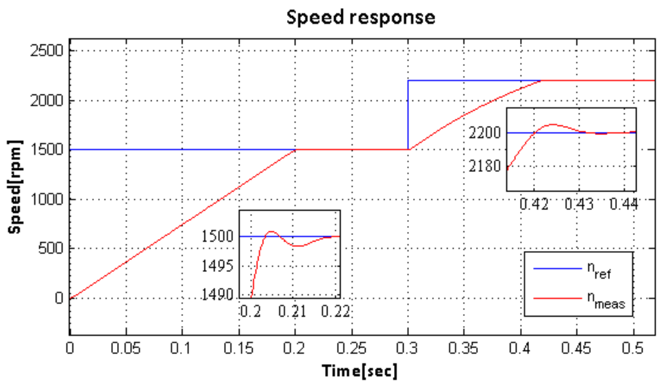

Figure 3.55: *Speed step response at 10Nm with FW*

After the motor stabilizes at 1500rpm, 10 Nm, at time t=0.3sec, a second step of 700rpm is applied. As it can be seen in Fig.3.56b, when the motor starts accelerating, the i_{s_d} current decreases, and is immediately limited by the imposed value of -212A. i_{sq} current is kept for a short time also at the maximum value of 212A. At this point the motor is providing the maximum torque.

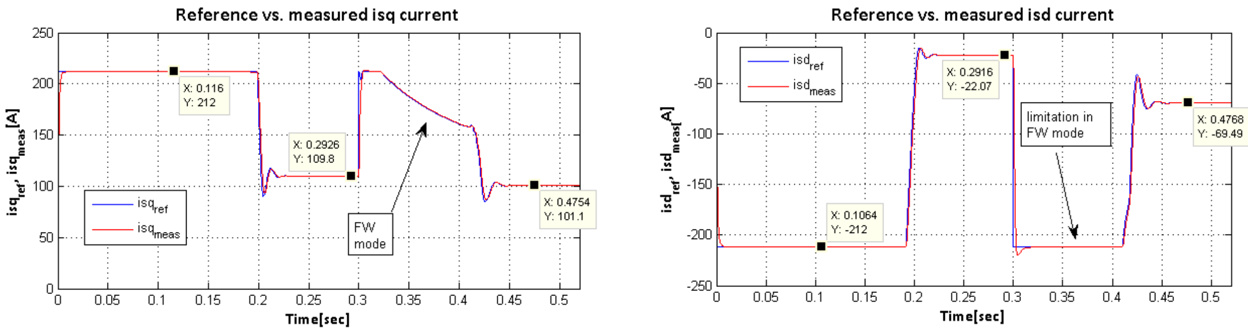

Figure 3.56: *Reference* dq *currents vs. measured* dq *currents*

The motor goes into field weakening when the q current starts to decrease,Fig.3.56a due to the fact that the modulation index has reached the threshold value, as it it presented in Fig.3.58 at time t=0.32. Due to the fact that the d current is limited, the acceleration torque cannot be kept at the maximum value and is decreasing as it can be observed on the torque curve in Fig.3.57.

When the speed reaches the set value, at 2200rpm, the motor reaches a steady-state point in FW, at a load of 10Nm. As it can be seen on the *dq* current curves, in Fig.3.56, at 10Nm in FW, the working point is lowered to (i_{s_d}, i_{s_q})=(-69.49, 101.1)A, compared to the previous steady-state point, at 10Nm.

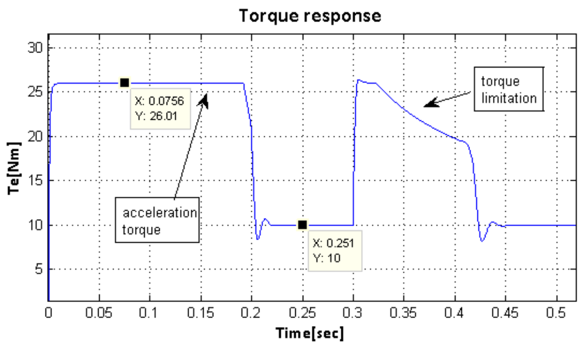

Figure 3.57: *Torque response at 10Nm load with FW*

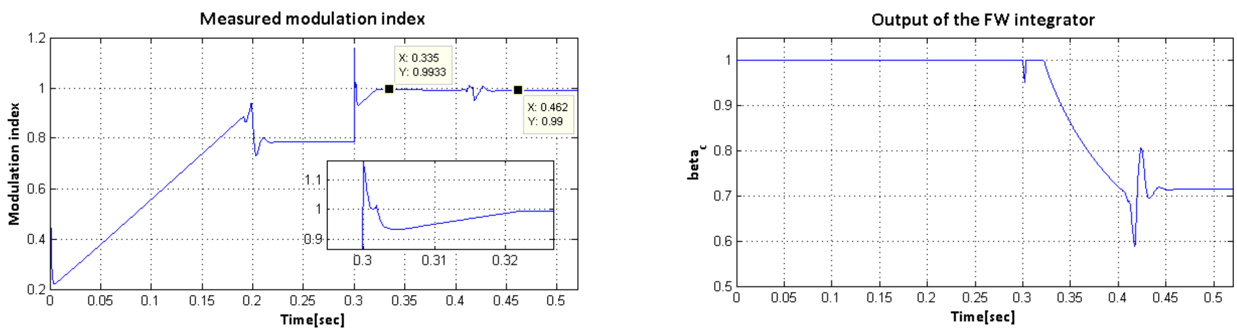

Figure 3.58: *Plot of a)the measured modulation index and b) the output β_c of the FW integrator*

A better visualization of the motor going into FW can be seen in Fig.3.59, where the locus of the stator phase current is plotted. At the start, the stator current follows route (1) to the maximum acceleration torque in point B(26Nm). The it follows the route (2)-(3) to reach a the steady state working point A, at 10Nm load. When the second speed step is given, the currents provide again the maximum acceleration torque, on route(4). After the measured modulation index exceeds the threshold value of M*=0.99, the motor goes into FW on route (5), in which i_{s_d} is limited. After the desired speed is reached, the stator current reaches a steady-state point(point C) in FW, along route (6). As it can be seen point A, which is out of FW, is on the same constant torque line, as point C, that is in FW.

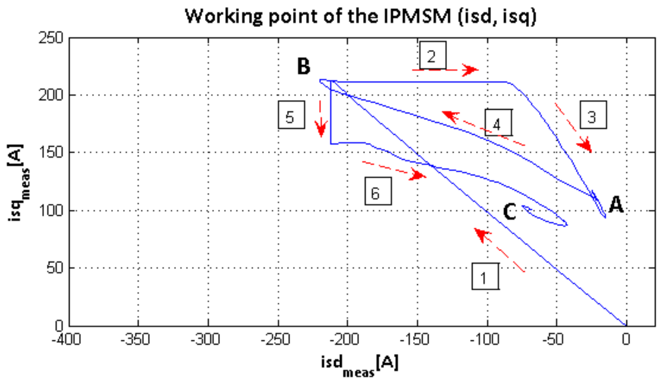

Figure 3.59: *Representation of the stator current vector*

Conclusion

In this chapter a Field Oriented Control strategy, capable of field weakening was presented and tested is a simulation model. The tests performed at different loads, with different reference speeds profiles, show that the implemented control is working with good results. Also from the results presented it was shown that the designed FW control is capable of preventing the saturation of the current controllers, when the motor goes into field-weakening. This is done by keeping the modulation index below 1.

Next step is to test the designed control in the laboratory. The control was implemented in a dSpace system. The test system, together with the results from the laboratory are presented in the next chapter.

4
Laboratory implementation

This chapter presents the laboratory implementation of the designed control system. In the beginning, a short description of the laboratory test setup is made. In the following the tests performed, and the results are presented. Conclusions are drawn at the end of the chapter

4.1 Laboratory test setup

The test setup on which the control was tested is presented in Fig.4.1.

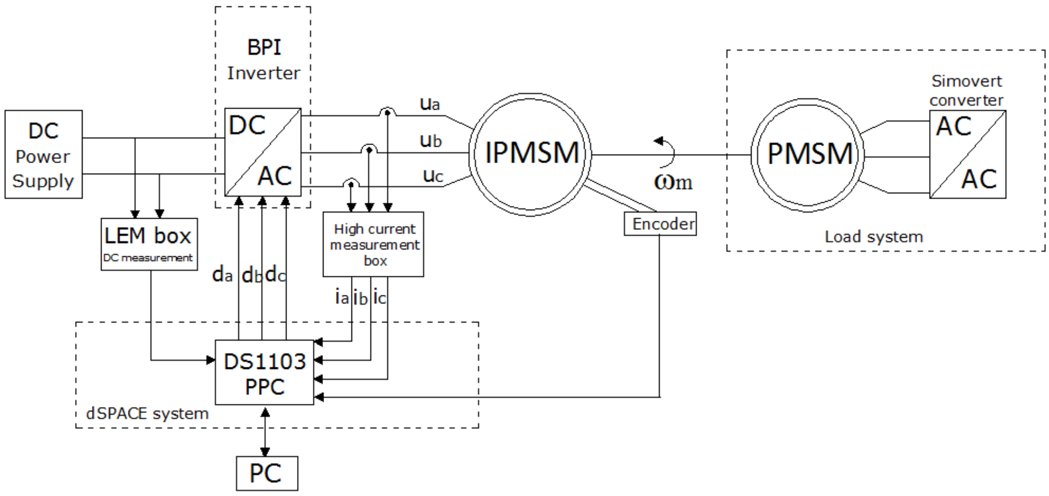

Figure 4.1: *Diagram representation of the laboratory test setup*

The main components of the system setup are:

- DC power supply
- BPI Sauer-Danfoss inverter
- dSpace control system
- Sauer Danfoss IPMSM
- loading system

- current and DC voltage measurement boxes
- encoder

The DC power supply is a LAMBDA EMI ESS Power Supply, capable of delivering maximum DC current of 330A, at a DC voltage of 32V. The inverter used is a BPI 5435 Sauer-Danfoss inverter tht has the following parameters:

- input 48VDC, -35%/20%
- output 0..32VAC, 0..350A

The main processing unit of the Dspace system is the DS1103 PPC digital controller. The DS1103 is a single board system that is based on the Motorola PowerPC 604e/333MHz processor (PPC). It features Matlab/Simulink as a software interface that allows all applications to be developed Simulink. All compiling and downloading processes are carried out automatically in the background. A software called Control Desk, allows real-time management of the running process by providing a virtual control panel with instruments and scopes.[Teodorescu,2003]

The Sauer-Danfoss IPMSM was presented in detail in Chapter 2. The loading system of the IPMSM consists of:

- the load motor that is a Siemens PMSM type ROTEC 1FT6084-8SH7 that has the following parameters:
  - rated power: 9.4 kW
  - rated torque = 20 Nm
  - rated current = 24.5 A
  - rated frequency = 300 Hz
  - rated speed = 4500 rpm.
- SIMOVERT converter system which is composed of a SIMOVERT RRU-regenerative line rectifier that provides the Dc-link to a SIMOVERT MC DC inverter; the Simovert inverter drives the PMSM load motor using a vector control strategy; the control strategy can have speed or torque as inputs.

In order to implement the control, the stator phase currents and the DC-link voltage of the inverter have to be measured. The DC-link voltage given by the DC supply to the inverter is measured using a LEM box, used in the dSpace laboratory, that has a voltage transducer. The conversion ratio of the transducer is 1/160. The high currents of the IPMSM are measured using a measurement box designed by students at IET, for a previous project in 2005. The current measuring box is equipped with LF 205 current transducers, that have a conversion ratio of 1/2000, and can measure up to 400A, peak.

The speed of the motor, needed in the control is measured using a standard Scancon, type 2R2500, incremental encoder, that has a resolution of 2500 pulses per revolution.

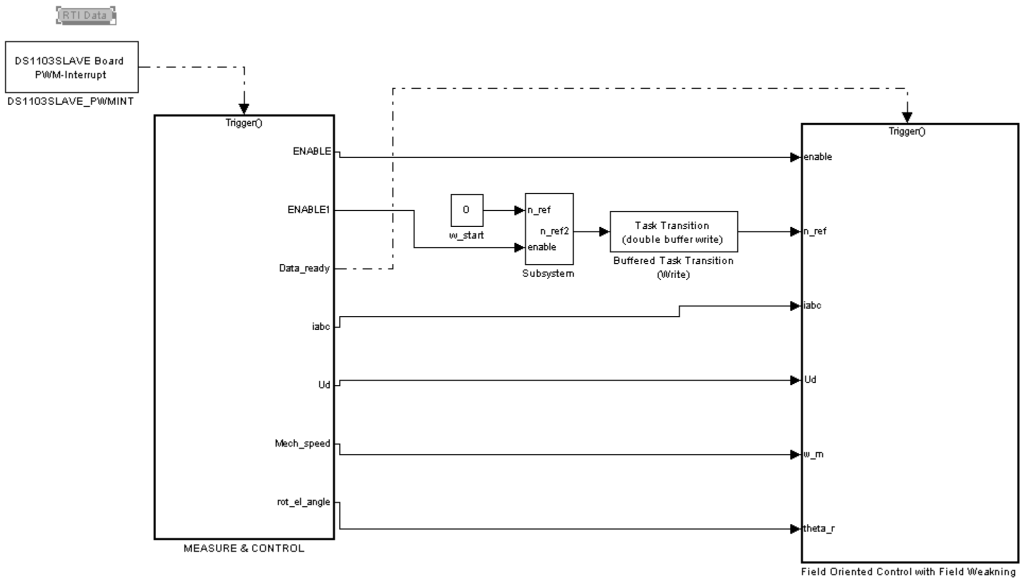

Figure 4.2: *RTI model*

RTI model The control designed in the previous chapter is introduced in a Real Time Interface(RTI) model, in Simulink. The model consists of two main blocks: *Measure and Control Block* and *FOC with FW block*, like presented in Fig.4.2.

The *Measure and Control Block* contains all the interface Simulink blocks for capturing the measured signals in the control, and also a protection block. This protection block provides software overcurrent protection, shortcircuit and overspeed protection. The *FOC with FW block* contains the actual discrete control presented in the previous chapter.

As it was mentioned before, Control Desk is used as a software for the real time management, and graphical visualization, of the process data. The layout designed for the control can be seen in Fig.4.3.

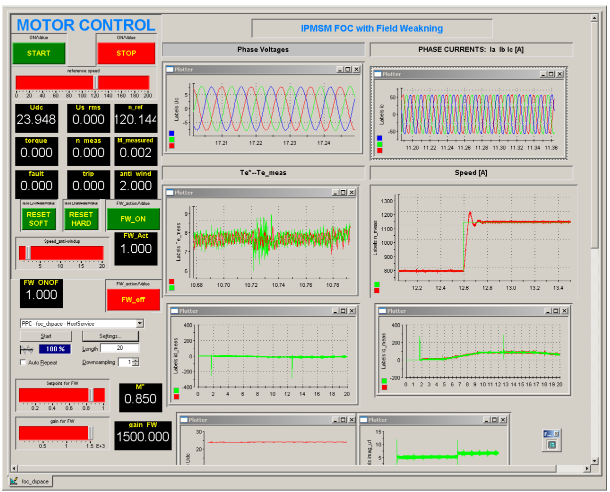

Figure 4.3: *Control Desk layout*

4.2 Results

In this section the tests performed in the laboratory are presented. As a first step the simple FOC structure was investigated, without field weakening. Then the FOC was tested with the FW control active. The parameters for the PI current and speed controllers used are the same as for the discrete controllers designed in Chapter 3. The anti-windup gains for the speed and current controllers used, have also the same value as presented in Chapter 3. The inverter switching frequency and also the sampling frequency is f=5kHz, the same as in simulation. The tests performed are the following:

- FOC test at no load
- FOC test at 5 Nm load
- FOC test with FW at 5 Nm load

4.2.1 FOC test at no load

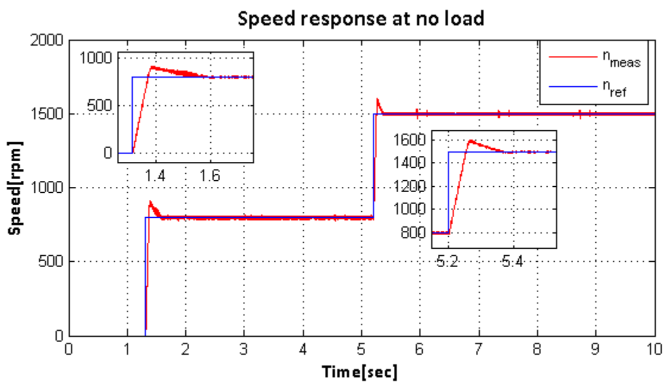

Figure 4.4: *Speed response at no load*

The first test presented is the test of simple FOC without field weakening at no load. The reference speed was set as a step of of 800 rpm, followed by a another step of 700rpm. The reference and the measured speed of the motor are presented in Fig.4.4. The speed response in both steps is characterized by a rise time of ≈ t=50ms, which is approximately the same as in the simulation results, at no load(t=60-70ms). Still, as it can be seen in the plot both steps have a maximum overshoot of 100rpm(12%).

The dq currents are plotted in Fig.4.5. During the acceleration time, for the both steps the currents are limited to the maximum value. This gives a maximum acceleration torque as presented in Fig.4.6. The torque value was estimated from the dq current measurement, based on the torque equation. During the two steady states, at 800 and 1500 rpm, the currents are not equal to zero, due to the fact that the machine has to produce a minimum torque to overcome the dry friction and the viscous friction. This can be seen also in the torque plot, where in steady state the torque is varying between 0.2-1.2Nm.

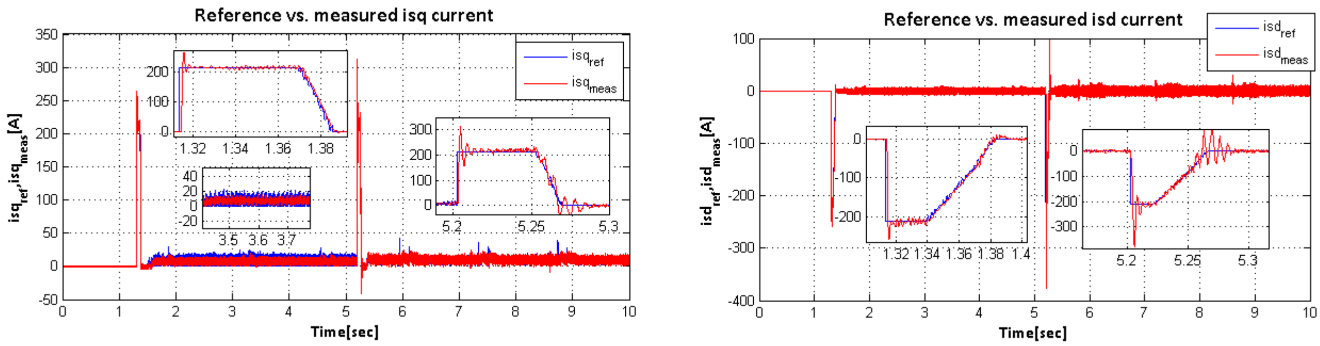

Figure 4.5: *Reference* dq *currents vs. measured* dq *currents*

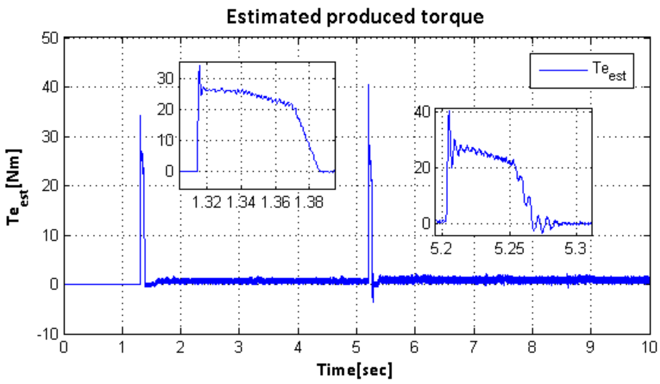

Figure 4.6: *Torque response at no load*

The real and imaginary components of the stator voltage are presented in Fig.4.7. In the two steady states the values of the dq voltages are (u_{s_d},u_{s_q})=(-1;5)V at 800rpm and (u_{s_d},u_{s_q})=(-3.5;8.5)V. This gives, for the two cases, an amplitude of the stator voltage of 5V, and 9V, that is almost the same as in the simulation model(4.8V and 9.15V).

The locus of the stator current amplitude is plotted in Fig.4.8. It can be clearly seen the locus of the maximum currents(that produce the maximum torque), and also the locus of the two steady states, where both currents are close to zero(zero torque). As the figure shows, the current vector follows approximately the same path during the two acceleration periods.

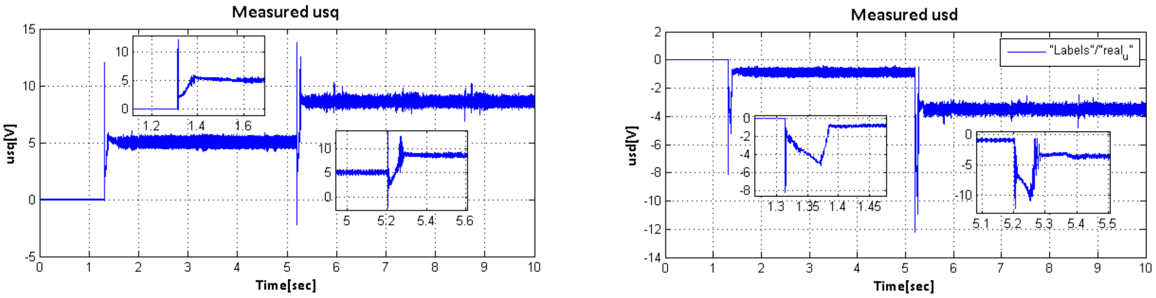

Figure 4.7: *Real and imaginary components of the stator voltage vector*

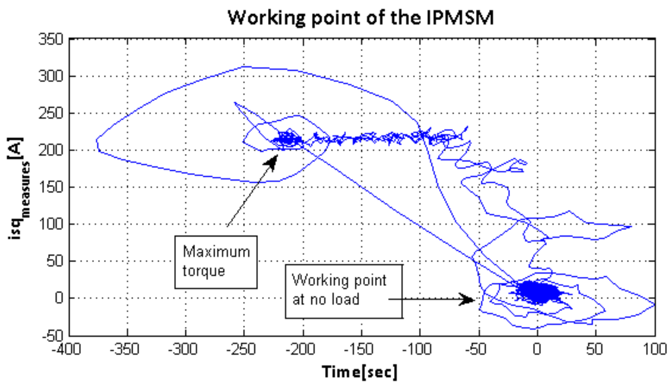

Figure 4.8: *Representation of the stator current vector*

4.2.2 FOC test at 5 Nm load

A second test was done for the simple FOC, without field weakening, but this time the motor was loaded. At the beginning the motor was started by a step of 800 rpm, at no load like for the previous test. At time t=4.7sec, a load of 10 Nm was applied. Due to the limitations of the loading machine, the load was applied as a ramp. After the load reached Tl=10 Nm, a second step was done until the final speed of 1150rpm. The plot of the reference and measured speed is presented in Fig.4.9.

The characteristics of the first step are the same as for the previous test. For the second speed step, while the motor was loaded, the rise time of the speed is approximately t=90ms. The rise time of this step is comparable with the results obtained in the simulation at 10Nm load. The maximum overshoot for this second speed step is ≈17%.

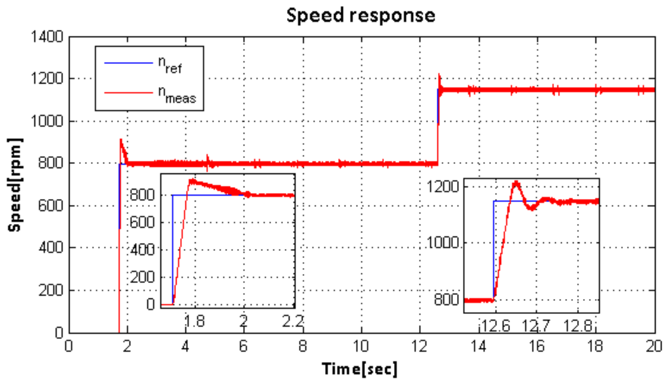

Figure 4.9: *Speed response at 10 Nm load*

The real and imaginary stator currents are plotted in Fig.4.10. After the load is applied at t=4.7sec, the i_{s_q} current starts to increase, following the ramp increase in the torque. The i_{s_d} current is also increasing, in absolute value. The working point at 10Nm load is:(i_{s_d},i_{s_q})=(-14;86)A, which is lower than the simulated working point(-22.7;109)A. This may be due to the difference between the real parameters of the machine and the parameters used in the simulation, or due to the load machine that is not providing the required torque.

When the second step in speed is made, the motor accelerates with the same maximum torque until it reaches the desired speed, as it can be seen in the estimated torque plot in Fig.4.11. After the speed stabilizes the dq currents stabilize in the same steady-state point.

The value of the torque at 10 Nm, is approximately 7.5Nm. The reason for this may be the same as for the currents.

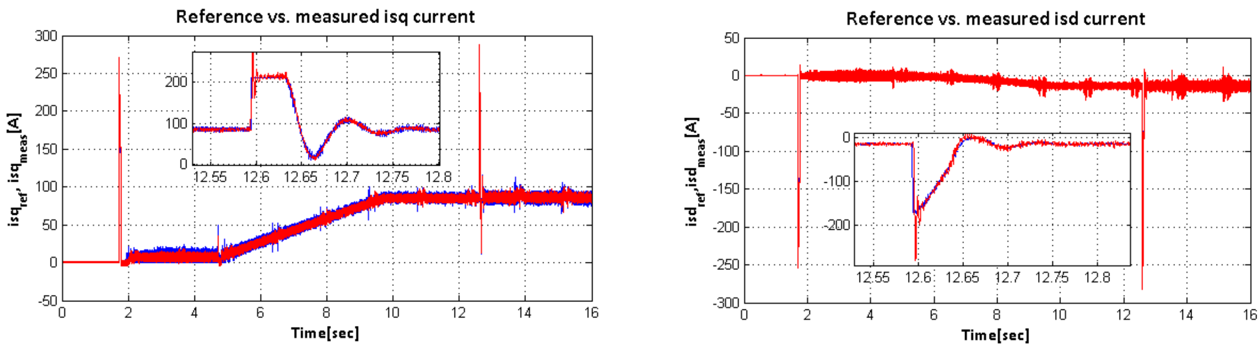

Figure 4.10: *Reference* dq *currents vs. measured* dq *currents*

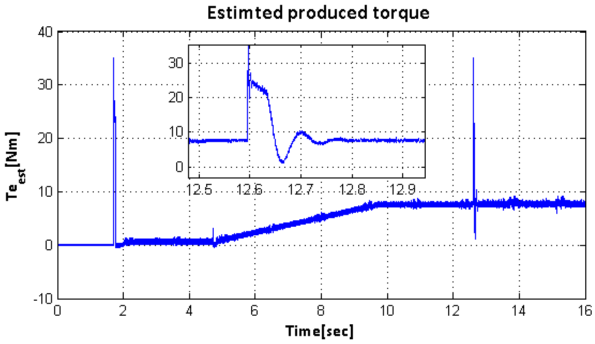

Figure 4.11: *Torque response at 10 Nm load*

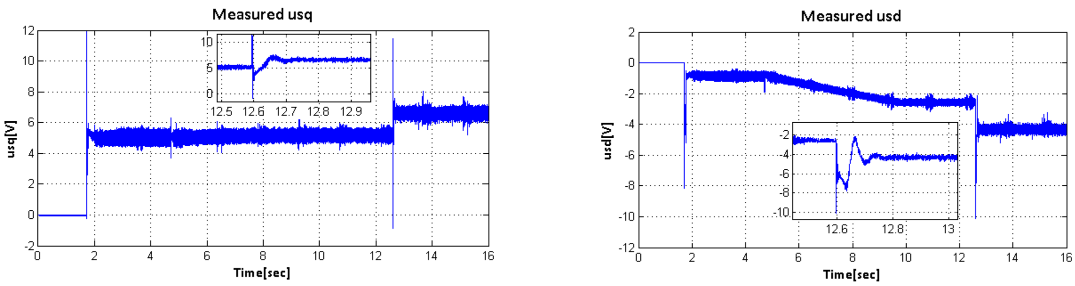

Figure 4.12: *Real and imaginary components of the stator voltage vector*

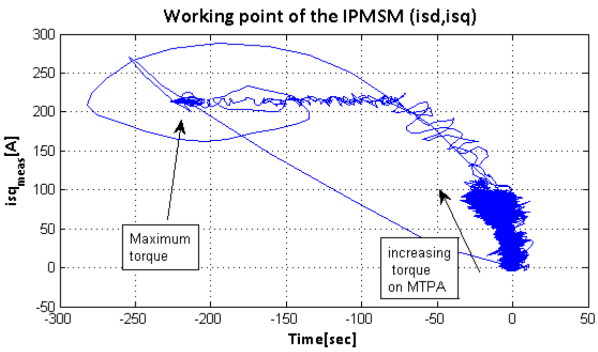

Figure 4.13: *Representation of the stator current vector*

The dq voltages are plotted in Fig.4.12. The value of the voltages at 800rpm, and 10Nm is (u_{s_d};u_{s_q})=(-2.6;5.2)V, that is almost the same with the simulated values for the same conditions (u_{s_d};u_{s_q})=(-2.8;5.6)V. For the second steady-state point the voltages are (u_{s_d};u_{s_q})=(-4.2;6.5)V

From the locus of the staor current vector, plotted in Fig.4.13, it can be seen the locus of the maximum currents, corresponding to the maximum torque, and also the rising of the vector on the MTPA curve when the load is increasing.

4.2.3 FOC test with FW at 5 Nm load

The FOC with FW was also tested in the laboratory. For this test the gain of the FW integrator was changed to k_{fw}=50. The threshold value of the modulation index was set to M*=0.5. The profile of the reference speed, and the measured speed are presented in Fig.4.14. The motor is started at no load with a step of 800rpm. After 3.7 seconds a load of Tl=5Nm is applied in a ramp. After a steady-state point is reached, another step until 1320 rpm is made. As shown in the speed plot, the measured speed follows the reference speed with good accuracy.

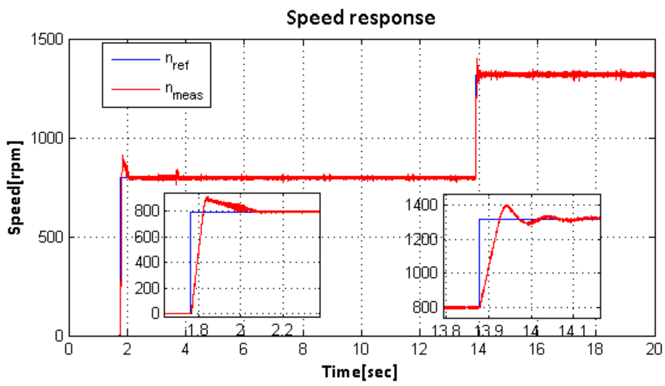

Figure 4.14: *Speed response with FW*

The real and imaginary components of the stator current are presented in Fig.4.15. As it can be seen on the i_{s_d} current plot, after the second speed step is made the motor goes into field weakening. The *isd* current increases in absolute value, towards the negative side while the i_{s_q} current approximately stays the same.

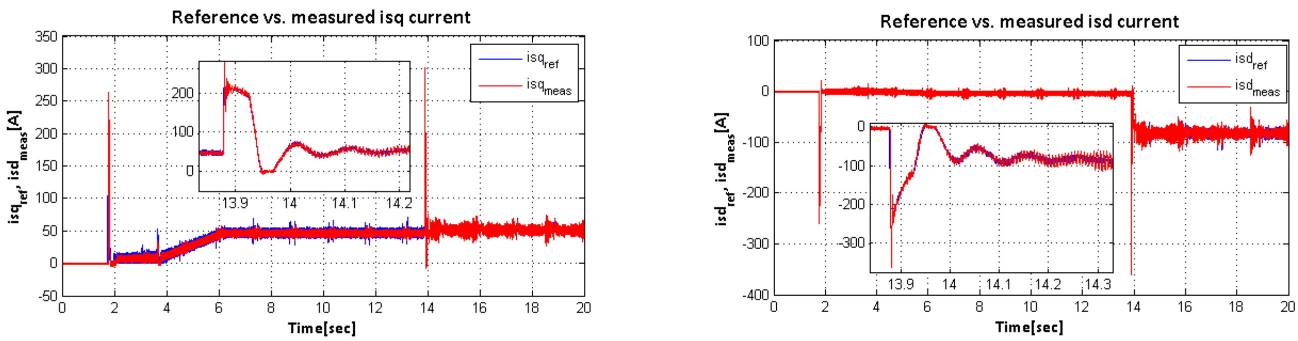

Figure 4.15: *Reference* dq *currents vs. measured* dq *currents*

A better visualization of the FW working point of the motor can be seen in Fig.4.16. After the motor reaches 800 rpm, it can be clearly seen that when the torque is applied the current vector moves along the MTPA curve. When the second step is made the motor goes into FW and stabilizes in a point approximately on the same constant torque curve, like shown in the figure.

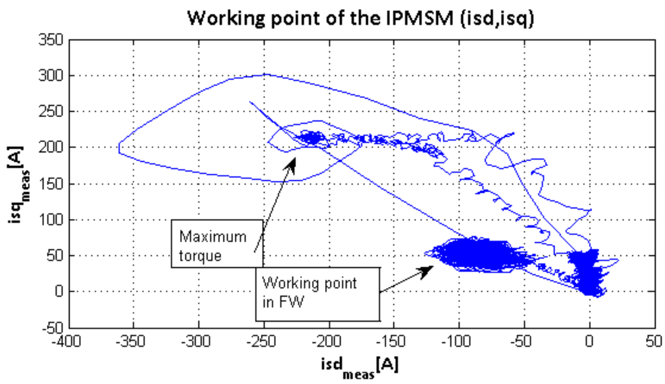

Figure 4.16: *Representation of the stator current vector*

The FW mode is triggered by the measured modulation index, as it can be seen in Fig.4.17. When the measured modulation index increases above the threshold value of M*=0.5, the output of the FW integrator starts to decrease. By this action the complementary angle of the stator current is lowered, and the motor goes into FW. The value of the output of the FW stabilizes, and the measured modulation index is kept at M=0.5.

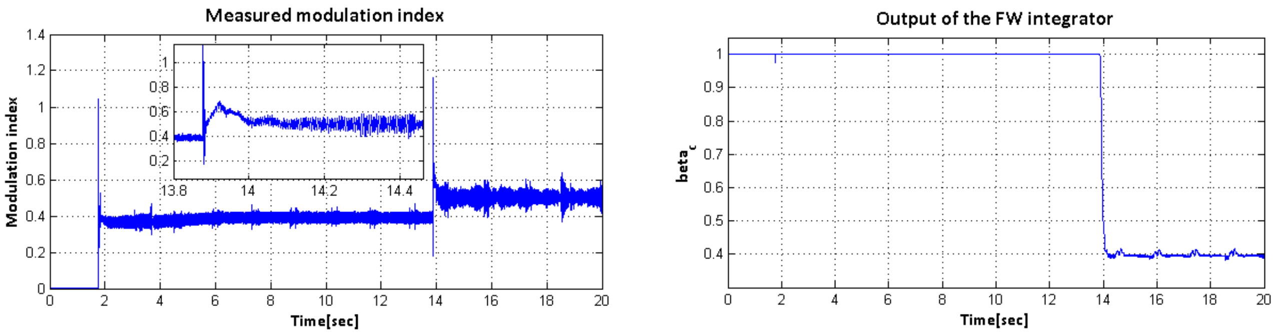

Figure 4.17: *Representation of the modulation index(a) and output of the FW integrator(b)*

In this chapter the experimental results are presented. Three test were performed: two tests with the simple FOC, without field weakening, at no load and with load, and a test of FOC with field weakening while the motor was loaded. The results presented show that the designed control for the FOC is working with good results. Considering the FW algorithm, the results presented show that the method chosen for FW is capable of running the motor in FW regime.

5 Conclusions

This project deals with torque control in field weakening mode applied to an interior permanent magnet synchronous motor. An indirect Field Oriented Control, with maximum torque per ampere control was designed and implemented in a Matlab/Simulink simulation model. The results from the simulation show that the method implemented is working with good results. Together with FOC, a Field Weakening control method was investigated, and implemented in the overall control system. From the presented simulated results it was shown that the FW algorithm, drives the motor into FW mode, with good speed and torque dynamics. The implemented FW method is capable of going into field weakening mode at constant torque.

The FW control is also capable of preventing the saturation of the current controllers, by keeping the measured modulation index M, bellow the value of 1. It was shown that when applying a ramp as reference to decrease the speed, the implemented method is capable of going out of FW, with constant torque. Still when a decreasing step was tried, to go out of FW, the speed of the motor becomes unstable. This is due to the choosing of the gain of the FW integrator, and the interaction between the action of the FW and the fast dynamics of the speed regulator.

Having the simulation model working, the designed control was implemented in a real-time system, in the dSpace laboratory. The FOC was tested at no load and with load. The results obtained from the experiments confirmed the simulation results, and showed that the FOC control implemented is working. The experiment performed with FW active proved that the FW control is capable of running the motor in FW mode, and the motor stabilizes in a working point on the constant torque curve.

Future Work

For future work the following tasks may be considered:

- For the MTPA control, instead of using the constant fixed values for the motor parameters, measurements can be done, in order to get the MTPA experimentally, and store the experimental data in the look-up tables for the MTPA

- The FW method should be tested at the maximum allowable voltage and current from the inverter, to validate the reliability of the method for all conditions; by this, also the maximum field weakening capabilities of the Sauer-Danfoss IPMSM could be evaluated

- Improve the FW controller so that it can also go out of FW when a step in speed is given

Bibliography

[ABB] Direct Torque Control, Technical Guide No.1, ABB

[Boldea,1999] I.Boldea, S.A.Nasar *Electric Drives*, CRC Press 1999

[Chandana,2002] P.D.Chandana Perera *Sensorless Control of Permanent-Magnet Synchronous Motor Drives*,IET Aalborg University, Ph.D. Thesis, Dec. 2002

[Ching,2005] Ching-Tsai P., Shinn-Ming S. *A Linear Maximum Torque Per Ampere Control for IPMSM Drives Over Full-Speed Range*, IEEE Transactions on Energy Conversion, vol.20, No.2, June 2005

[Franklin,2006] G.F. Franklin, J.D.Powell *Feedback Control of Dynamic Systems- Fifth Edition*, 2006 ISBN 0-13-149930-0

[Jahns,1986] T.M.Jahns G.B.Kliman *Interior Permanent-Magnet Synchronous Motors for Adjustable-Speed Drives*, IEEE Transactions On Industry Applications, Vol. IA-22, No. 4, Jul/Aug 1986

[Jahns,2001] J.Wai, T.M.Jahns *A New Control Technique for Achieving Wide Constant Power Speed Operation with an Interior PM Alternator Machine*,2001, IEEE

[Jonas,2006] J.Ottosson, M.Alakula *A Compact Field Weakening Controller Implementation*, SPEEDAM 2006 International Symposium on Power Electronics, Electrica Drives, Automation and Motion

[Kazmierkowski] M.P.Kazmierkowski, H.Tunia *Automatic Control of Converter-Fed Drives*, Warszawa 1994

[Mizera,2005] R.Mizera *Modification of Symmetric Optimum Method*, ASR 2005 Seminar, Instruments and Control, Ostrava, April 29, 2005

[Morimoto,1990] S.Morimoto, Y. Takeda *Expansion of Operating Limits for Permanent Magnet Motor by Current Vector Control Considering Inverter Capacity*, IEEE Transactions on Industry Applications, Vol.26, No.5, Sept/Oct1990

[Ogata,1997] K.Ogata *Modern Control Engineering*, 3rd Edition, 1997

[PED8] *Sensorless Control for PMSM*, PED8 semester project, Group PED-817, Aalborg University, spring 2003

[PED9] *Control of a variable speed variable pitch wind turbine with full scale power converter*, Group PED-9,Aalborg University, December 2007

[Soong,1994] W.L.Soong, T.J.E Miller *Field-weakening performance of brushless synchronous AC motor drives*, IEE Proc-Electr. Power Appl., Vol. 141, No. 6, November 1994

[Sul,2003] B-H Bae, S-K Sul *New Field Weakening Technique for High Saliency Interior Permanent Magnet Motor*, Industry Applications Conference, Oct.2003,ISBN: 0-7803-7883-0

[Teodorescu,2003] R.Teodorescu*Getting started with dSPACE system*, Aalborg University, Institute of Energy Technology, Department of Electrical Energy Conversion, Version 2003

[Wu2006] B.Wu *High-Power Converters and AC Drives*, IEEE Press, 2006

Summary

The project *Torque Control in Field Weakening Mode*, is a proposal from Danfoss. The main idea of the project is to control the speed and torque of an Interior Permanent Magnet Synchronous Machine(IPMSM) in the flux weakening regime, considering the voltage and current limits of the inverter.

The first chapter begins with a short introduction into the Field Weakening mode of an IPMSM. The main features of this control are presented, taking into account also the inverter that is feeding the machine. Next the Problem formulation and the Objective of this project are stated. In the end of the chapter, the limitations and the structure of the report are presented.

In the second chapter, at the beginning a classification of the Permanent Magnet machines is made. Then the main characteristics of the Interior type permanent magnet motor are presented, together with the electrical parameters of the IPMSM used in this project. Next the mathematical model of the IPMSM is presented. Based on the mechanical model of the machine, a dynamic simulation model is made using Matlab/Simulink. In the end of the chapter the measurements made to calculate the mechanical parameters of the machine and the results from the simulation model are presented.

In Chapter 3, the implementation of the Field Oriented Control(FOC), together with the Field Weakening(FW) algorithm is presented. Starting from the general topology of FOC, the Maximum Torque per Ampere(MTPA) control is presented, and also the tuning of the PI parameters. Next the FW algorithm chosen is presented. In the end the overall simulation model is presented, together with the simulation results.

In Chapter 4 the laboratory implementation of the designed control system is presented. In the beginning of the chapter, a short description of the laboratory test setup is made. In the following the tests performed, and the results are presented. Conclusions are drawn at the end of the chapter.

The final chapter, Chapter 5, presents the conclusions of the project and the future work.

A

Initialization file

```
%Torque Control in Field Weakening Mode for IPMSM

%IPMSM Parameters

Rs = 0.00962 ;%[OHMS] stator resistance
Lsd = 28.7e-6; %[H] d component inductance
Lsq = 47.2e-6; %[H] q component inductance
Psi_m = 9.71e-3; %[Wb] PM flux linkage
pb = 6 ;% nb. of pole pairs
J =20.17e-3;  % moment of inertia
B =0;% viscous friction coeficient
f_sw=5e3; %Switching=sampling frequency
T_sw=1/f_sw; %Sampling time
Ts=T_sw
Udc=24

%Discrete controllers parameters

%speed loop
kpw_d = 0.8404;
kiw_d = 105;

% q current loop
kpiq_d = 0.0471;
kiiq_d = 9.6;

% d current loop
kpid_d = 0.0289;
kiid_d = 9.65;

% Continuous Current controllers parameters

% iq current loop
kp_iq = 0.0471;   % 0.061
```

```
ki_iq = 9.6122;   %11.727

%id current loop
kp_id = 0.0289;
ki_id = 9.6333;

%Speed loop controllers
kp_w=0.8404
ki_w=105.05;
```

B
File for generating MTPA curve

```
% This program creates id*=f(Te*), iq*=f(Te*) for MTPA control of an IPMSMS
%input  parameters
Psi_m = 0.0097;
pb = 6;
Ld = 2.8700e-005;
Lq = 4.7200e-005;
Isn = 300;
k=1;

for is=0:0.1:Isn
    p=[2 Psi_m/(Ld-Lq) -is*is];
    R=roots(p);
    if(R(1)<R(2)), id=R(1);
    else
        id=R(2);
    end
    iq1=sqrt(is*is-id*id);
    Te1=1.5*pb*(Psi_m+(Ld-Lq)*id)*iq1;
    Vid(k)=id;
    Viq1(k)=iq1;
    VTe1(k)=Te1;
    i=is;
    k=k+1;
end
M1=[VTe1;Vid];
M21=[VTe1;Viq1];
plot(Vid,VTe1,'-',Viq1,VTe1,'-r')
```

C
Simulation model

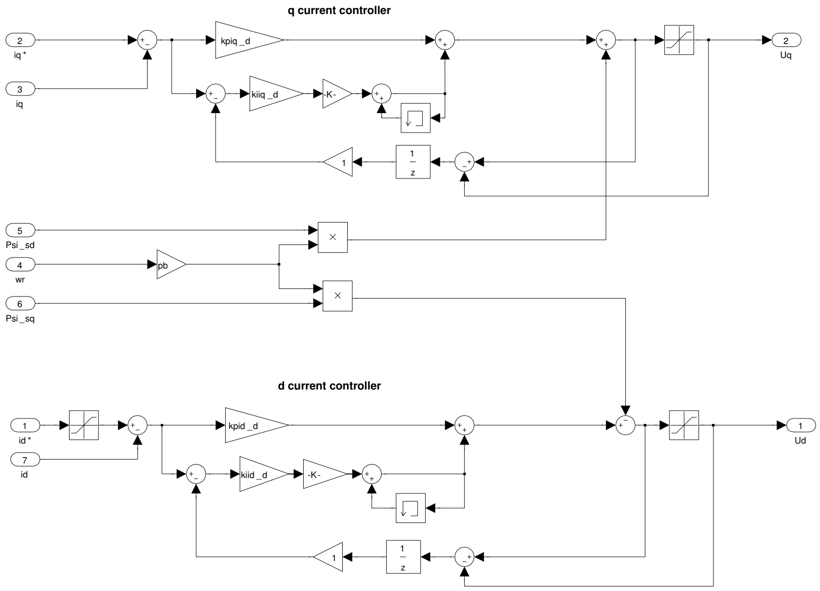

Figure C.1: *Simulation model of the current controllers*

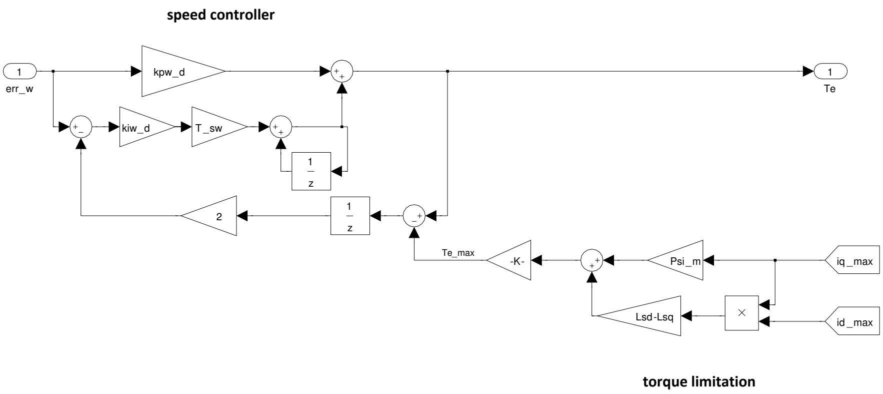

Figure C.2: *Simulation model of the speed controller*

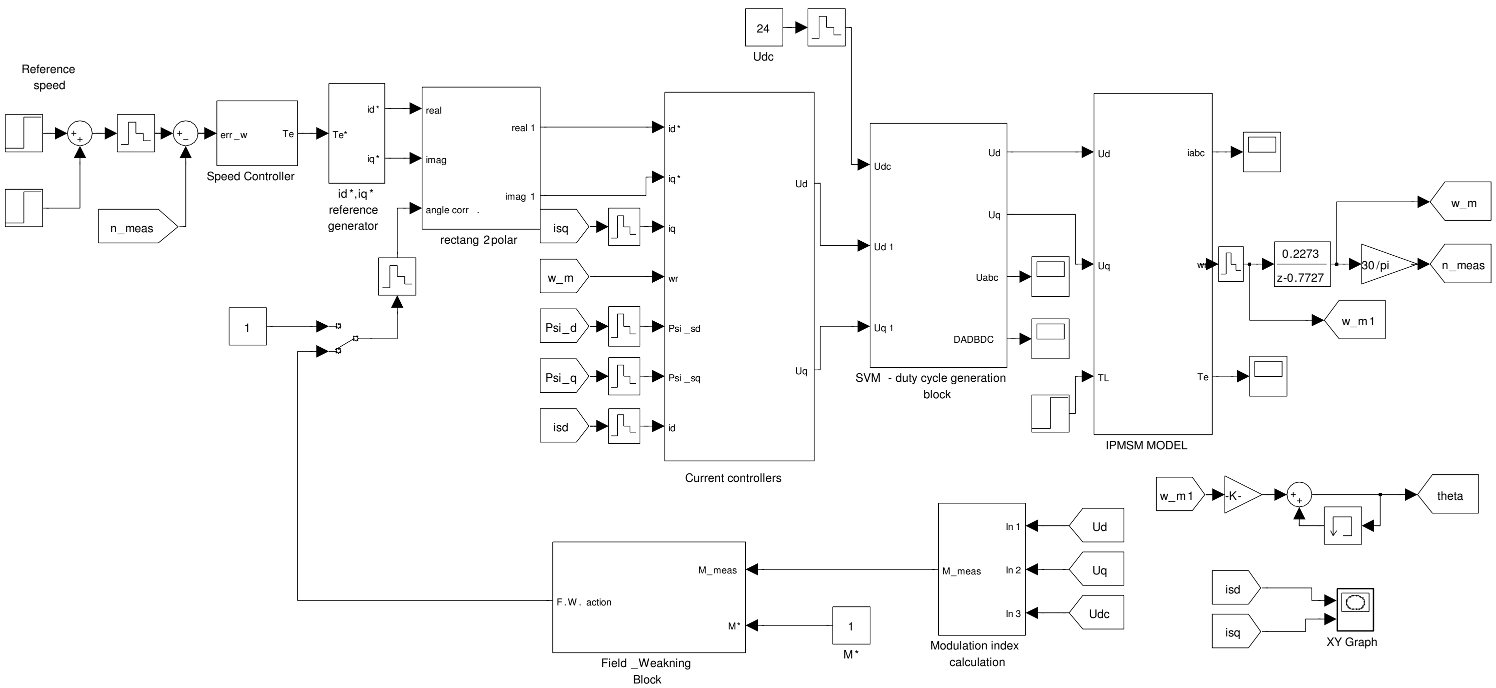

Figure C.3: *Overall simulation model*